AFRPシートで曲げ補強したRC梁の耐衝撃挙動に関する実験的研究

Experimental Study on Impact-Resistant Behavior of RC Beams Strengthened in Flexure with Externally Bonded Aramid Fiber-Reinforced Polymer Sheets

By

LE HUY SINH

A DISSERTATION SUBMITTED TO THE FACULTY OF THE MURORAN INSTITUTE OF TECHNOLOGY IN PARTIAL FULFILLMENT OF THE REQUIREMENTS FOR THE DEGREE OF DOCTOR OF ENGINEERING

Division of Civil and Environmental Engineering
MURORAN INSTITUTE OF TECHNOLOGY
September 2022

ACKNOWLEDGMENTS

I would like to express my sincere gratitude to my supervisor, Professor Dr. Masato Komuro, Chair of the Laboratory of Structural Mechanics, for his ongoing support of my research, for granting me permission to conduct this research, and for his expert guidance, fruitful discussions, and helpful suggestions made throughout the course of this research.

The author would like to express their gratitude to the Japan Society for the Promotion of Science (JSPS) KAKENHI Grant Number JP17K06527 for funding my PhD program and assisting me in completing this study.

I also want to express my gratitude to the members of my doctoral dissertation examination committee, Associate Professor Noriyuki Sugata, Professor Mitsuo Mizoguchi, and Specially Appointed Professor Norimitsu Kishi, for their insightful comments and helpful suggestions that helped me improve the caliber of my dissertation.

I would like to sincerely thank Dr. Tomoki Kawarai for supporting me with expertise and working conditions while studying and living in Muroran.

I would like to express my sincere thanks to all staff at the Center for International Relations, Muroran Institute of Technology staff. Especially, Ms. Hatsuki Noda has supported my family and me with the best living conditions so that I could study and research with peace of mind.

The author also thanks to all students of the Laboratory of Structural Mechanics for their assistance during this study.

I am appreciative of Dr. Duong Quang Hung's introduction and endorsement of Professor Masato Komuro and Muroran Institute of Technology before I applied for the PhD program here.

I want to express my gratitude to Associate Professor Dr. Dang Vu Hiep and Dr. Dao Minh Hieu for their assistance with my application for this course.

The Vietnamese community in Hokkaido and my overseas friends are also appreciated. They have assisted me greatly by studying, living, and working here.

Additionally, I would want to express my gratitude to Associate Professor Dr. Le Anh Dung and Associate Professor Dr. Vu Hoang Hiep of Hanoi Architectural University for providing me with letters of recommendation so that I could apply for this PhD program. I also thank the Division of Construction and Construction Machinery, Faculty of Civil Engineering, Hanoi Architectural University for creating the ideal conditions for my study and research at Muroran Institute of Technology.

Finally, I would like to sincerely thank my wife, Mrs. Tran Thi My Hanh, my son, Le Tung Lam, and my daughter, Le Tran Khanh Linh, for all of their love, support, and patience while I was conducting my research in Japan. I want to convey my sincere gratitude to my mother, my wife's parents, and the Vietnamese relatives who have helped and supported me. I would not have been able to finish this research without their ongoing assistance.

TABLE OF CONTENTS

LIST OF TABLES

LIST OF FIGURES

ABSTRACT

Traditional techniques, such as steel plate bonding, section expansion, and external post-tensioning, have been employed to reinforce or retrofit old concrete structures. However, these methods have drawbacks such as raising the weight of the structure, being challenging to install, and having the reinforcing material corrode, resulting in increased maintenance costs. Corrosion resistance, a high strength-to-weight ratio, and ease of installation are just a few of the amazing benefits of fiber-reinforced polymer (FRP) materials. These characteristics have led to a significant amount of research and the use of FRP materials with carbon, glass, aramid, and basalt fibers in civil engineering. For the most part, FRP materials were used to reinforce RC beams in flexure and/or shear under static loads. There are design guidelines that are frequently used for externally bonded FRP systems to reinforce concrete structures. However, current global terrorist threats and activities have significantly threatened civil infrastructure, necessitating the building of blast and impact-resistant structures. In order to enhance RC constructions against static, blast, and impact loads, FRP materials can be employed. Studies on RC beams with FRP reinforcement that can withstand impact loading, however, are scarce. Design guidelines for RC members under impact loading have not yet been developed.

This paper focuses on RC beams with stirrups that exhibit flexural failures and approach the ultimate state statically. To examine the strengthening effect and failure mode of the RC beams, low-velocity drop-weight impact loading tests on RC beams reinforced in flexure with Aramid FRP sheets were carried out with varying drop heights of the weight (0.5, 1.0, 2.0, 2.5, 3.0, and 3.5m) and sheet volume (415, 830, and 1660 g/m^2). The impact-resistant properties of the RC beams were also investigated in the experiments including successive impact loading with progressively increasing energy. Here, sheet volumes of 415, 830, and 1660 g/m^2 were employed. The weight's drop height was raised to the equivalent ultimate state of the beam in increments of 1, 2, 2.5, and 3 m. Static loading studies on the RC beams were also performed to examine the load-carrying capacity, strain distribution, crack distribution, and failure behavior of the beams. The outcomes were contrasted with impact loading testing, multilayered technique calculations, and the previous study's failure mechanism. The following are the study's conclusions based on the experimental results: (1) Depending on the volume of the sheet, the failure mechanism of the reinforced RC beams with AFRP sheets was divided into

two types: flexural compression failure and debonding failure. These findings are consistent with the prior investigation. (2) In the event of impact loading (with a single loading method), the maximum and residual displacement of the strengthened beams can be restrained by up to 35% and 85%, respectively, in comparison to unreinforced beams. (3) The maximum/residual deflections of the RC beams, whether they had AFRP sheets or not, rose linearly with the input impact energy. (4) Based on the volume of the sheet, the rupturing and debonding failure modes of the reinforced RC beams were distinguished. The former relates to the failure mode known as flexural compression, whereas the latter relates to the failure mode known as debonding under static loading. (5) In the case of successive drop-weight impact loading, the reinforced beams' absolute maximum/residual deflections were linearly distributed with the total input impact energy, and the failure mechanism of RC beams tended to be the same as in the case of a single impact loading.

Chapter 1: INTRODUCTION

1.1 General background

Significant issues for structural engineers include strengthening and retrofitting reinforced concrete (RC) structures. Most civil infrastructure is typically overloaded, which can result in structural deterioration due to insufficient load-carrying capacity. Retrofitting RC members must take overload into account. Additionally, to satisfy the demands of the service load, the old structures that were erected several decades ago may need to be renovated and reinforced. In the realm of retrofitting, a number of techniques for strengthening RC members with different materials, such as steel plate bonding, section expansion, and external post-tensioning, have been researched and used. However, these methods have drawbacks, including heavier structures, installation challenges, and corrosion of the reinforcing material, which raises maintenance costs. Materials made of fiber-reinforced polymer (FRP) have a number of exceptional benefits, such as resistance to corrosion, a high strength-to-weight ratio, and ease of installation. These characteristics have led to a large number of studies and applications on FRP materials made of carbon, glass, aramid, and basalt fibers in the field of civil engineering. There are established and often used design guidelines for externally bonding FRP systems to reinforce concrete structures [1]. The RC structures are strengthened using near-surface mounted FRP bars and externally bonded FRP sheets.

Civil infrastructures face enormous challenges as a result of global terrorist threats and activities, necessitating the building of structures with explosion and impact resistance. FRP materials can therefore be employed to improve RC constructions' resistance to static, blast, and impact loads. There are, however, limited investigations [2,3] on strengthening RC structures that have been subjected to blast loads. There have only been a small number of prior studies on FRP-enhanced RC beams resistant to impact loads [4]. There are currently no design guidelines for RC structures subject to impact loading.

From this perspective, low-velocity drop-weight impact loading tests on RC beams strengthened in flexure with Aramid FRP (AFRP) sheets were conducted. The goal of these tests was to analyze the effects of the sheet volume and weight drop height on the failure mode of the beams. Additionally, to examine the impact-resistant qualities of the RC beams strengthened with FRP sheets, successive drop-weight impact loading tests with progressively more energy were conducted. The load-bearing capacity, strain

distribution, crack distribution, and failure behavior of the beams were also studied using static loading experiments. The results of these studies were compared to impact loading tests and calculated results to verify the criteria of failure mode of strengthened beams compared to the prior research.

1.2 Objectives and scope of research

The objective of this study is to improve a practical flexural reinforcing technique for impact-resistant RC beam reinforcement using externally bonded AFRP sheets. This investigation focuses on RC stirrup beams that flexural fail when they approach the ultimate state statically.

This study's goal is divided into two main sections:

- Drop-weight impact loading tests with a single loading method were first carried out to evaluate the impact-resistant behavior of RC beams strengthened in flexure with AFRP sheets under impact loading. Investigations were done into how the sheet volume and input impact energy affected the beams' failure mechanism. The sheet volume ranged between 415 and 1660 g/m^2. A 300 kg steel weight was dropped from a variety of heights (0.5, 1.0, 2.0, 2.5, 3.0, and 3.5 m) until the sheets were ruptured or debonded, which produced the impact force. Chapter 5 will have a detailed presentation of this section.

- Consecutive drop-weight impact loading experiments on RC beams reinforced in flexure with externally bonded AFRP sheets were carried out to evaluate the impact-resistant properties of the RC members for the second goal. To assess the strengthening effect of beams, the sheet volume and cumulative input impact energy were examined. 415, 830, and 1660 g/m^2 sheets were utilized. Up until the matching ultimate state of the beam, the weight's drop height was incrementally increased in the order of 1, 2, 2.5, and 3 m. In Chapter 6, this section will be presented.

The load-carrying capacity, strain distribution, crack distribution, and failure behavior of the beams were also studied using static loading experiments. The results of these studies were compared to impact loading tests, calculated results, and the findings of earlier studies to confirm their accuracy. Chapter 4 will include a description of this section.

1.3 Thesis outline

The organization of the seven chapters that make up this thesis is depicted in Figure 1.1.

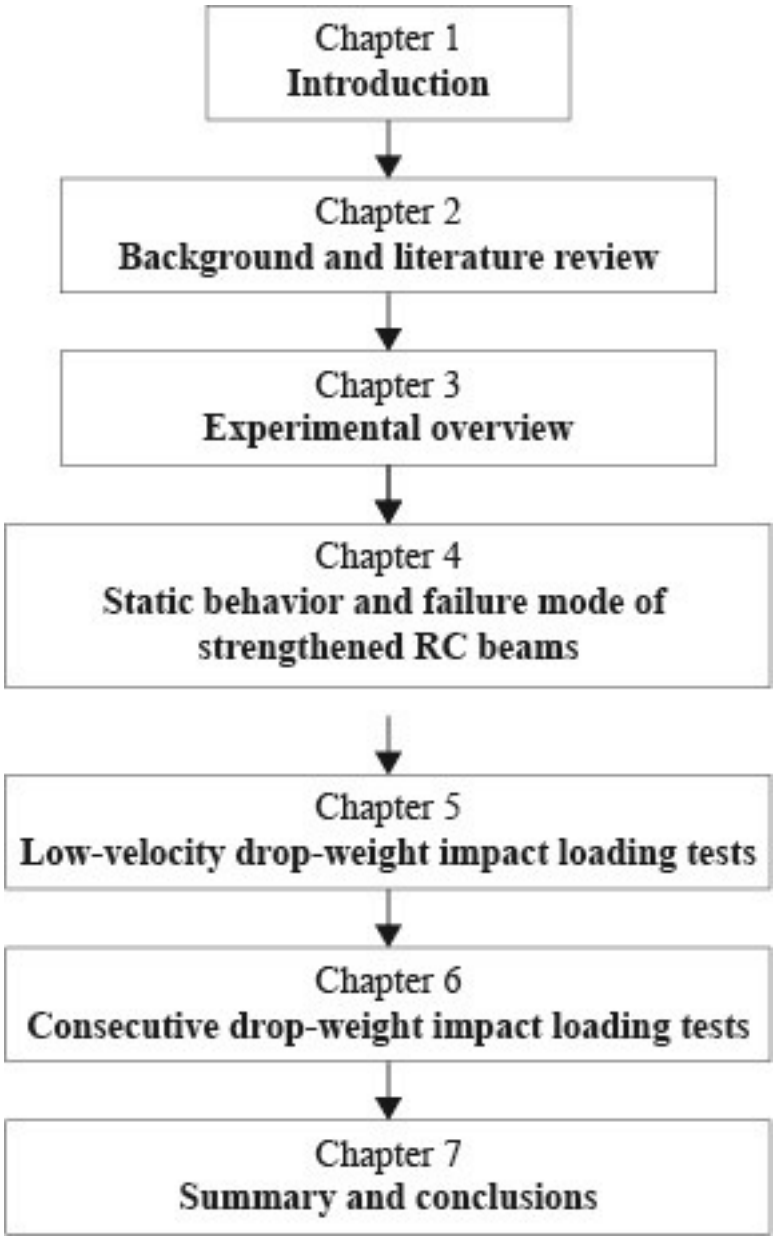

Figure 1.1. Flow chart of a dissertation.

Chapter 2: BACKGROUND AND LITERATURE REVIEW

2.1 Introduction

Materials made of fiber-reinforced polymer (FRP) have a number of exceptional benefits, such as resistance to corrosion, a high strength-to-weight ratio, and ease of installation. These characteristics have led to numerous studies and uses of FRP materials in civil engineering. Design guidelines for using externally bonded FRP systems to reinforce concrete structures have been created and are being widely used [1]. Externally bonded FRP sheets and FRP bars positioned close to the surface are the two strengthening techniques that are typically used to reinforce the constructions.

The literature on using FRP materials to strengthen or retrofit RC structures under static and impact loading is compiled in this chapter. The reinforcing procedures and material properties of FRP materials also are described briefly.

2.2 Design methods for strengthening RC members with externally bonded FRP systems

2.2.1 FRP sheet bonding method

According to reference [1], the most popular approach for strengthening reinforced concrete structures is known as externally bonded reinforcement (EBR). In this procedure, following surface preparation, epoxy was used to adhere FRP sheets or laminates to the tension face of the concrete member. In order to improve concrete's ability to adhere, surface preparation seeks to clean out impurities and polish the surface. The enhanced control beams are RC beams that have been strengthened using the EBR approach. Variables like the number of layers and bond length of the FRP sheet/laminate were used. Figure 2.1 provides an illustration of the EBR approach.

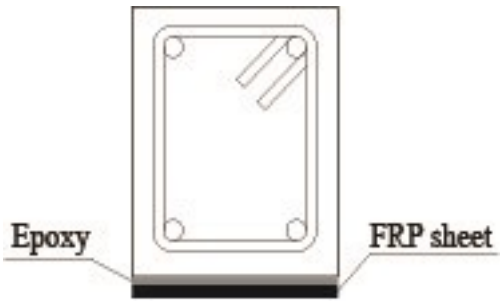

Figure 2.1. EBR technique.

This method has advantages and disadvantages [5] as follows:

Advantages of this technique are:

1) Fast and simple installation;

2) Low operating expenses;

3) Immediate usage of strengthened structures; and

4) Absence of need for specialized labor skills.

Disadvantages of this technique are:

1) Brittle failure mode brought on by premature debonding of the FRP sheet from the concrete substrate;

2) Vulnerability of FRP materials to environmental factors like freeze/thaw cycles, abrasion, mechanical impacts, acidic and alkaline environments, fire, vandalism, and UV radiations; and

3) Changes brought on by the structure's appearance.

Fast, simple installation and affordable implementation are this method's standout benefits. Furthermore, if the surface preparation of the bonded concrete is handled thoroughly, the bond between the sheet and the concrete substrate is regarded as excellent. Then, the premature sheet debonding phenomenon can not occur. Therefore, this method has been applied most commonly among externally bonded techniques.

Studies and applications of FRP materials for strengthening/repairing RC members by FRP sheet/laminate bonding method will be presented in detail in section 2.4 of this chapter.

2.2.2 FRP rod near-surface mounting method

FRP sheet bonding and/or tension-side surface overlaying with concrete have both been utilized to reinforce existing RC structures. The concrete surface of the strengthened part will, however, be perfectly covered with a sheet and/or overlay of concrete employing such methods. The following drawbacks have been identified as a result of the findings: 1) it is impossible to visually inspect a crack that has developed as a result of concrete deterioration; 2) the anti-fatigue capacity of existing concrete tends to be decreased as a result of undrained water infiltrated concrete; and so on.

Near-surface mounted (NSM) technology was designed to utilize more of the tensile strength of the FRP material before failing as a result of debonding failures in externally bonded FRP strengthening systems. The NSM method only requires one step: sawing a groove into the concrete surface and filling it partially with two-part structural

epoxy. An FRP rod or strip is subsequently inserted into the groove, which has now been completely filled with epoxy resin, as shown schematically in Figure 2.1. The use of NSM FRP rods and strips is taking the place of externally bonded FRP laminates. The ability to anchor the bars/strips into adjacent members, as well as a quicker installation time and a more appealing completed appearance, are all advantages of adopting NSM systems. This strengthening method is mentioned in reference [1] of Chapter 1.

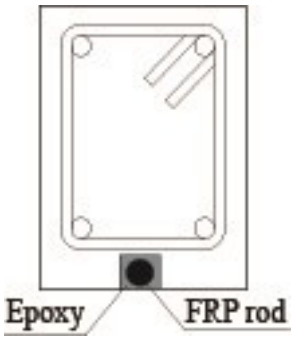

Figure 2.2. NSM technique.

This strengthening method has advantages and disadvantages [5] as follows:

Advantages:

1) A reduction in the strengthening process since surface preparation is not necessary;

2) Delay or even abolition of the debonding phenomena;

3) The ability to preserve FRP materials against abrasion makes this technology applicable to the negative moment zone of flexural frames;

4) Making pre-stressing of strengthening materials easy;

5) protecting reinforcement materials against harsh environmental factors such as mechanical impacts, abrasion, fire, freeze/thaw cycles, vandalism, and UV radiation; and

6) The use of different FRP materials, such as hand-made FRP rods, strips, and rods, is conceivable.

Disadvantages:

1) Time-consuming and expensive installation process; and

2) The effects of the grooving process on the environment.

From the above advantages, the NSM method has been widely applied in practice. Here are some typical applications:

In order to investigate the strengthening effects of near-surface mounted (NSM) FRP rods on the impact-resistant capacity of reinforced concrete (RC) beams, Kishi et al.

[6] conducted static and falling-weight impact tests on the RC beams while controlling for the FRP rod material and weight-falling height. In this case, AFRP and CFRP rods were taken into consideration. Impact testing was carried out utilizing a single loading method and a 300 kg mass of weight. These trials' findings were as follows:

Static loading test:

1. Flexural strengthening with NSM FRP rods can logically improve the RC beam's rebar yield point and static load-carrying capacity, and the upgrading impacts of both materials are nearly the same; and

2. The FRP rod debonded under the probing action of the diagonal crack tip, causing the beams to attain their final state.

Impact loading test:

3. Regardless of the size of the input impact energy, the configurations of the time histories of the impact force, the response force, and the midspan deflection of the FRP rod NSM RC beams were nearly identical;

4. The FRP rod NSM RC beams exhibited an impact-resistant behavior that was almost identical when the input impact energy was low;

5. The rods used to reinforce the beams with NSM CFRP rods attained their ultimate condition because they broke and debonded with less force than those used to strengthen them with AFRP rods;

6. The rods used to reinforce the beam with NSM AFRP debonded under the peering action of the diagonal fracture, bringing the beam to its final state; and

7. As a result, the upgrading effects of the AFRP rods on the beams' capacity to withstand impacts may be greater than those of the CFRP rods.

In an experimental investigation, Sharaky et al [7] assessed how RC beams reinforced with NSM FRP bars behaved. Eight beams were assessed using four-point bending. All of these factors—material type, epoxy characteristics, bar size, and NSM bar count—were looked into. The grooves could only be cut all the way up to the faces of the supporting columns, thus the tested beams were reinforced with a short bond length to as closely mimic workplace conditions as feasible. The tested beams' load carrying capability, deflection, failure mechanism, FRP strain, concrete strain, free end slip, and transverse strain in the epoxy and concrete were all examined. For beams strengthened utilizing CFRP and GFRP, respectively, the yielding loads of the strengthened and control beams increased by 155.8% and 129.8%, while the ultimate loads increased by 166.3% and 159.4%. Beams strengthened with CFRP bars were stiffer than those reinforced with

GFRP bars. The size, shape, or quantity of bars in the epoxy had little effect on the strengthened beams' capacity to support loads; instead, epoxy failures and concrete cover separation were the main causes of failures.

Khalifa [8] tested six full-scale RC beams that had been strengthened using various CFRP techniques. These beams are intended to fail flexurally. The performance and efficacy of the NSM and EBR procedures for the flexural strengthening of RC beams were compared in his research. The results of the tests showed that, while using the same amount of CFRP, beams strengthened with NSM strips outperformed those strengthened with EBR in terms of ultimate load. The ultimate load ratio increased by this amount between 12% and 18%.

The effectiveness of reinforcing RC beams with pre-stressed NSM-CFRP systems was examined by Lee et al. [9]. In their study, eight RC beams were put through four-point loading tests, with an un-strengthened control beam serving as the standard. The final three beams were strengthened using post-tension NSM-CFRP bars, while the final four beams were strengthened with pre-tension NSM-CFRP bars. The test findings demonstrated that relative to the control beam, strengthening with a pre-stressed NSM beam improved the beam's flexural behavior. The post-tension NSM systems improved beam performance for the concrete cracking, steel yielding, and ultimate loads the best.

Insufficient shear reinforcement was found in fourteen beams that were evaluated under four-point bending by Al Rjoub et al. [10]. In this work, the impacts of side concrete cover depth, NSM-CFRP strip inclination angle, and NSM-CFRP strip length on the behavior of RC beams were investigated. Six beams were cast with three different side concrete cover depths, 20, 30, and 40 mm, and were strengthened in shear by NSM-CFRP, with inclination angles of 0° and 45°. Other beams with side concrete cover depths of 30 mm were strengthened in shear by NSM-CFRP with various strip lengths, measured in beam depth (full, 2/3, and 1/3), and inclinations of 0° and 45°. The outcomes demonstrated that the depth of the concrete side cover improved the behavior of NSM-CFRP strengthened beams. The ultimate strength of beams with inclined NSM-CFRP strips was higher than that of beams with vertical NSM-CFRP, and it was discovered that ultimate strength increases with longer strip length.

In their research on the global flexural performance of RC beams reinforced internally with CFRP rods utilizing the Side Near Surface Mounted (SNSM) approach, Abdallah et al. [11] presented an experimental program that had been carried out. In precut grooves, the CFRP rods were inserted laterally next to the longitudinal steel bars.

The primary variables examined in this study were the length, position, and kind of filler material for CFRP rods. The SNSM and NSM procedures for the strengthening of RC beams employing CFRP rods were also thoroughly compared in order to validate and evaluate the efficacy of the SNSM technique. Their research has shown that while the SNSM-CFRP rod approach increased the load-bearing capacity of RC beams, it also reduced their ductility and deflection at maximum load. Additionally, the results showed that the filler material's properties and the length of CFRP rods had an impact on the failure mechanism. The strengthening position did not, however, make a big difference at the same time. An alternative to the NSM approach is the SNSM strengthening procedure. It might be utilized in some situations to stop non-traditional failure modes brought on by the NSM strengthening system deterioration, like the early failure of debonding or the pulling out of CFRP rods.

The efficiency of NSM rope and strip in the shear strength of RC beams was experimentally examined by Saadah et al. [12]. A total of fifteen RC beams with dimensions of 150 mm x 250 mm x 1200 mm (width x height x length) were built and tested. To analyze the load-displacement behavior of RC beams strengthened by NSM Rope and Strip FRP, the following characteristics were taken into consideration in each configuration: CFRP orientation angle, the spacing between CFRP, and the strengthening scheme. Based on their findings, reinforced concrete beams can be strengthened using NSM-CFRP rope. In comparison to all other configurations, using inclined CFRP ropes or strips has the highest load-carrying capability. Depending on how far apart the CFRP was, the maximum load capacity rose by (150–170%) from the control specimen. In the strengthened specimens, flexural shear failure has replaced brittle shear failure due to the inclined NSM-CFRP ropes or strips.

Experimental and numerical analysis was used by Imjai et al. [13] to study the flexural performance of low-strength RC beams reinforced with NSM-CFRP rods. Up until failure, four-point bending tests were performed on five RC rectangular beams. Using Bottom NSM (BNSM) or Side NSM (SNSM) rods, four of these beams were strengthened. The findings showed that the beams' cracking load was increased by up to 19% by the SNSM strengthening solution. The yield and ultimate load-carrying capacities of the reinforced beams also improved, rising by up to 31% and 64%, respectively. It is further demonstrated that between 20% and 10% of accuracy at failure, moment-curvature, and FE techniques accurately estimate the deflections of the strengthened RC beams. Up to failure (within a 10% accuracy), the nonlinear Finite Element (FE) analyses

had a greater agreement with the experimental findings. The fracture widths predicted by Eurocode 2 for the beams examined in this study agree with the measured values to a fair extent.

In an experimental study, Cho et al. [14] examined how a system of NSM-CFRP bars could improve the flexural performance of RC beams that had aged poorly. In order to discriminate between old and new concrete, different steel reinforcement ratios, different amounts of prestressed and non-prestressed CFRP bars, and ten 6.4 m long RC beams were constructed and tested in four-point bending. According to their findings, the NSM-CFRP strengthened RC beams had ultimate strengths that were up to twice as high as those of the control beams that weren't strengthened, and the strengthening effect grew stronger as the RC beam's material properties changed.

Despite being a modern technique, NSM delivers a high level of strengthening efficacy, is less likely to have a premature debonding failure, and improves defense against fire, mechanical damage, the effects of aging, and vandalism. Due to the reinforcement's internal location, the approach also exhibits improved durability, stress-sharing mechanisms, and fatigue performance. However, serviceability criteria in terms of overall deflections and crack widths, rather than delamination of externally bonded FRP reinforcement, control the constraints of adopting NSM-FRP reinforcing bars and strips. In order to get around the drawbacks of traditional strengthening methods, various researchers have developed innovative ways of combining EBR and NSM. In this chapter's section 2.4, the references will be listed.

Because it is quick and simple to deploy, the EBR approach was used for this study. Under static and impact loading, this technique was used to reinforce RC beams with AFRP sheets.

2.3 FRP materials and matrix resins

2.3.1 FRP material properties

Combining two or more materials, each of which has distinct qualities from the others produces composite materials. An FRP composite is composed of fibers, resins, interfaces, fillers, and additives. The high elastic modulus of the fiber improves the mechanical properties of FRP. While preventing mechanical and environmental degradation, resins help transfer stresses from one fiber to another. It is well known that the behavior of FRP composites is influenced by the interface between the fibers and matrix. Fillers, in addition to the three main ingredients, assist in lowering cost and

shrinkage. The physical, mechanical, and workability characteristics of composites are all enhanced by additives. The four main substances utilized to create fibers for the civil engineering sector are, order, CFRP, glass (GFRP), AFRP, and basalt (BFRP) (see Figure 2.3). Figure 2.4 illustrates the stress-strain relationships between steel reinforcement and FRP.

FRP composites, as opposed to steel, are impervious to chloride-induced corrosion because of their structurally non-corrosive and non-metallic characteristics, which could greatly increase structure corrosion resistance. Table 2.1 displays the mechanical properties of steel and other FRP material types. In contrast to regular steel, FRP is lightweight and highly durable. Although this, its mechanical characteristics are linear elastic with no obvious yielding stage, resulting in lower failure strain and elongation rates. With the exception of CFRP, which has a high Young's modulus, FRP frequently has an elastic modulus that is lower than steel. FRP composites that could be used as concrete reinforcement include roving, rebar, rod, tube, sheet, beam stirrup, plate, textile, and mesh fabric. Steel rebars manufactured by pultruding impregnated thermoset resin fibers could be replaced by FRP bars, such as those depicted in Figure 2.3, which provide promise.

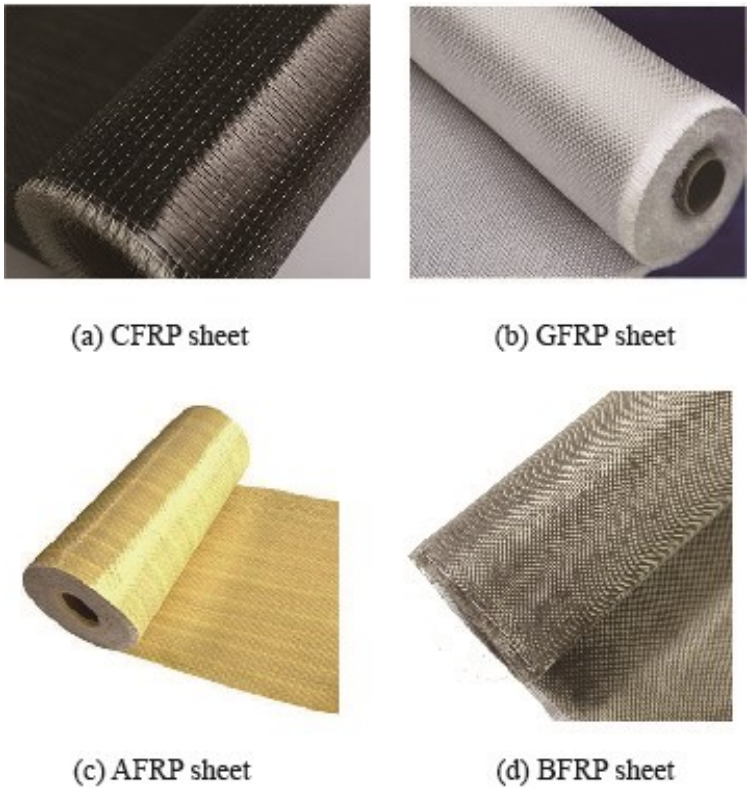

Figure 2.3. Typical types of FRP sheets.

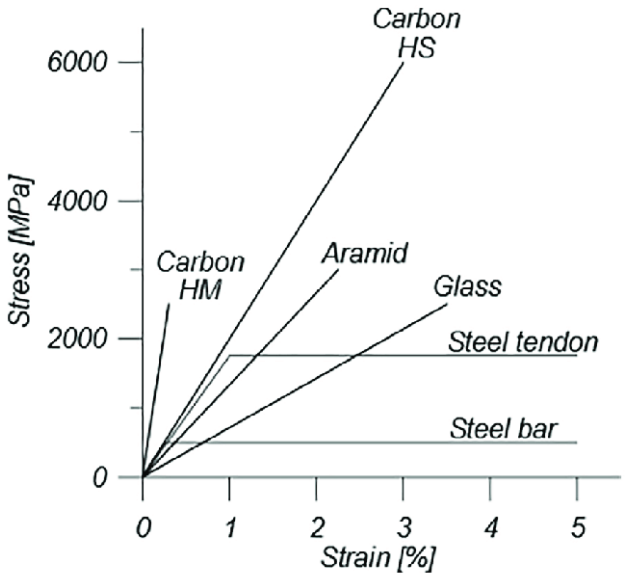

Figure 2.4. Stress-strain relationships between materials [15].

Table 2.1. Comparison of basic physical and mechanical properties between FRP bars and steel bars [16].

Property	Material type				
	CFRP	GFRP	AFRP	BFRP	Steel
Density (gm/cm^3)	1.50–1.6	1.25–2.10	1.25–1.40	1.90–2.10	7.85
Tensile strength (MPa)	600–3690	483–1600	1720–2540	600–1500	483–690
Young's modulus (GPa)	120–580	35–51	41–125	50–65	200
Elongation (%)	0.5–1.7	1.2–3.1	1.9–4.4	1.2–2.6	6.0–12.0
Coefficient of linear expansion (10^{-6}/^{o}C)	–9.0–0.0	6.0–10.0	–6.0–2.0	9.0–12.0	11.7

2.3.2 Types of FRP fibers

2.3.2.1 Carbon Fiber Reinforced Polymers (CFRP) material

Anisotropic carbon fiber is a naturally occurring compound that is created at about 1300 degrees Celsius. Among its main attributes are low density, low conductivity, high fatigue strength, high elastic modulus, good creep level, chemical resistance, and the lack

of water absorption. However, because it is anisotropic and has a low compressive strength, carbon fiber (has lower radial strength). Another disadvantage is that producing carbon fiber requires a lot of energy, which raises the price [17].

2.3.2.2 Glass Fiber Reinforced Polymers (GFRP) material

A typical isotropic filament is glass fiber. E-glass, S-glass, C-glass, and AR-glass are the most prevalent types of glass fibers. Glass fiber's strong strength, resistance to water and chemicals, and low cost make it essential. Due to its low cost when compared to other types of FRPs, glass fiber is the most commonly utilized FRP in the construction sector. On the other hand, glass fiber has a low elastic modulus, is alkaline resistant, and has a low long-term strength because of stress rupture. When better alkaline resistance is needed, the alleged AR-glass may be utilized [17].

2.3.2.3 Aramid Fiber Reinforced Polymers (AFRP) material

Aramid fiber is yellow and anisotropic. Kevlar is the name given to aramid fiber on the market. Although more expensive than glass fiber, aramid fibers are ideal for tension applications like tendons and cables despite having poor compressive strength. This substance is light in weight and has high tensile strength, high elastic modulus, and adequate stiffness. Both static and impact structures can use this fiber. Due to the limited radial strength and long-term strength (stress rupture), its usefulness is restricted. Cutting and processing aramid fiber is difficult. Examples of numerous Kevlar variants with various qualities include Kevlar-29, Kevlar-49, Kevlar-149, Technora H, Twaron, and Twaron HM [17].

2.3.2.4 Basalt Fiber Reinforced Polymers (BFRP) material

A type of volcanic rock known as basalt fiber is created when lava on a planet's surface rapidly cools. Basalt fiber can be produced similarly to glass fibers, and the only raw materials required are crushed basalt rocks. Basalt fibers are a relatively new addition to structural materials and FRP composites. These fibers offer high tensile strength, great heat resistance, and exceptional durability (Table 2.1). Excellent electromagnetic properties, as well as resistance to corrosion, acid, radiation, UV rays, and vibration, are further benefits. The use of BFRP in the field of civil construction is fairly limited when compared to FRP composites manufactured from glass, carbon, and aramid fibers [17].

2.3.3 Matrix resins

To create sheets and bars, depending on the kind of FRP, the fiber is mixed with a matrix of resin, fillers, and additives (Figure 2.5). Resin is the primary component of a matrix. Thermosetting resins and thermoplastic polymeric materials are the two different types of resins. The first is utilized more frequently for creating FRP composites. Unlike thermoplastic polymers, once hardened thermoset polymers cannot be reheated or molded. Thermoset possesses exceptional stiffness, dimensional and thermal stability, and resistance to electrical, chemical, and solvent effects despite its normal brittleness. Keeping the fibers together, transferring the weight to the fibers, and shielding them from outside impacts are the main objectives of a matrix [17].

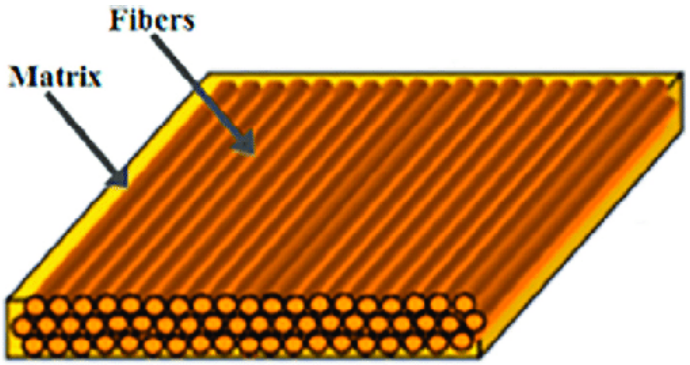

Figure 2.5. Typical composite geometry of FRP [17].

2.3.3.1 Epoxy resin

It is a very diverse class of artificial resin. As it advances, it might be used as an adhesive, coating, flux, casting plastic, and matrix resin for FRPs used in building applications. The epoxy resin is remarkably versatile given its decreased shrinkage and ease of manufacture. The epoxy resin typically outperforms thermoset polyester in terms of characteristics and, when used with the right hardeners, exhibits good heat and chemical resistance, particularly to alkalis. The best mechanical properties, corrosion resistance, adaptability, and durability of epoxy resins make them the most popular substrates for many researchers [17].

2.3.3.2 Vinyl ester

As a thermosetting polymeric matrix in FRP composites, this thermosetting resin could be utilized in place of epoxy and polyester resins. It is halfway between epoxy and polyester in terms of strength, characteristics, and overall prices. Vinyl ester resin is less

viscous (about 200 cps) than epoxy (around 900 cps) and polyester (roughly 500 cps). Due to its anti-corrosion properties and capacity to resist water absorption, it is a resin that is frequently used in the marine industry. According to BS4994, the vinyl ester is predominantly used as a resin to create FRP tanks and vessels. It improves strengths and mechanical properties more than polyester resins but less than epoxy. Vinyl resin is commonly used in laminating and repairing products because of its dependability and waterproofing [17].

2.3.3.3 Polyester

Due to its low cost, anti-corrosion, quick curing, ease, and temperature tolerance, polyester resin is frequently utilized in FRP composites. It does, however, have significant drawbacks, such as a low elastic modulus and only a (5–15)% improvement. A creep could also result from polyester. Compared to conventional epoxy resin, which contains (3.5-4.5)%, polyester exhibits tensile elongation at a break of about (1-2)%. The low cost of polyester resin makes it desirable, however, the saturated environment of vinyl ester resin makes it the preferable choice [17].

2.4 Studies and applications of FRP materials for strengthening/repairing RC members

2.4.1 Studies and applications of FRP materials for strengthening/repairing RC members under static loading

FRP material is preferred over conventional materials because it is lightweight, corrosion-resistant, has a high strength-to-weight ratio, and is simple to install. Therefore, since the 1990s, FRP applications in civil engineering have been encouraged. On 16 under-reinforced beams, Ritchie et al. [18] examined the efficacy of external strengthening employing FRP plates in the early 1990s. The tension side of the beams was attached using plates made of glass, carbon, and aramid fibers. They discovered that the FRP-plated beams had stiffness increases (across the operational load range) of 17 to 99% and strength gains (ultimate) of 40 to 97%.

RC rectangular and T-section beams strengthened by attaching glass FRP plates to tension flanges were also examined by Saadatmanesh and Ehsami [19] for improvements in static strengths. Tests for four-point bending failure on five rectangular beams and one T-beam were conducted. In accordance with the experimental findings, bonding GFRP plates to the tension face can greatly boost the flexural strength of RC beams. Epoxy-

bonded plates additionally enhanced the beams' cracking behavior by delaying the onset of cracking and decreasing fracture widths under increased loads.

Triantafillou [20] assessed the use of CFRP laminates as shear strengthening materials for RC beams and the contributions of FRP materials to the shear load-carrying capacities of beams using both experimental and analytical methods.

To create a sensible flexural strengthening method for RC elements reinforced with FRP sheet, Kishi et al. [21] conducted static loading tests on RC beams reinforced with AFRP sheet. The following factors were changed for creating the sixteen various types of strengthened RC beams: rebar ratio (0.8, 1.2, and 1.8%), shear span ratio (3.1, 4.0, 5.0, 6.0, and 6.9), and sheet volume ratio (1.0 and 2.0%). The investigations demonstrated that 1) There are two failure modes (sheet debonding failure and flexural-compressive failure), with the mode being dictated by the rebar yield length. 2) The sheet gradually debonds as a result of concrete exfoliation on the bottom cover concrete of the equi-shear span. 3) Using a fiber model, it is possible to strengthen the design of flexural-failure-type RC beams with a margin of safety.

The application of FRPs on RC beams was investigated mathematically and experimentally by Kishi et al. [22]. The goal of their research was to create a numerical analytic technique that would replicate the load-carrying capacity of RC beams that failed in the FRP sheet peel-off mode. In this case, geometrical discontinuities such as cracks opening, rebar slippage, and FRP sheet debonding were taken into account using the discrete crack technique. Analytical and experimental results comparisons showed that the suggested numerical analysis method was suitable for determining the load-carrying capacity and failure behavior of flexurally reinforced RC beams with an FRP sheet.

Ahmed et al. [23] examined the transverse bending failure of six reinforced concrete beams with varying degrees of strengthening schemes across an effective span length of 1900 mm. By changing the layers of composite laminates, the ultimate strength gain offered by bonded carbon fiber was assessed. The findings demonstrated that the flexural strength of the beams dramatically increased as the number of laminate layers increased. The test found no indication of the overlaid CFRP plates delaminating. However, debonding of CFRP laminates from the concrete surface was seen in the multi-layer beam strengthening situation. It was determined that the performance of CFRP reinforced beams was greatly impacted by the attachment of CFRP laminates to edge strip plates. Additionally, the various stages of the strengthening scheme's failure mechanisms for the beam were underlined.

Seven reinforced concrete beams with flexural strengthening were put to the test utilizing a four-point bending device by Attari et al. [24] in order to complete the failure analysis. To determine how effective external strengthening systems for reinforced concrete beams using FRP fabric are, various strengthening configurations are taken into consideration (use of separate unidirectional glass and carbon fibers with some U-anchorages or of bidirectional glass-carbon fiber hybrid fabric) (Glass–Carbon). Their research revealed that strengthening reinforced concrete beams with a twin layer glass-carbon fiber composite material was particularly effective. Comparing the reinforced beam specimens to the reference control specimen yielded a strength capacity increase of 114%, yet without a significant loss in ductility. The reference specimen, on the other hand, saw a noticeable deformation of the hybrid strengthening arrangement with a ductility ratio of 0.9. Additionally, by causing more severe deformations in the beam specimens, the U-anchorage strengthening configuration increased flexural strength and helped redistribute internal pressures. The finest outcomes were produced by this setup. Additionally, the results showed that, in comparison to other strengthening configurations, using a strengthening composite material in glass fibers alone or as a single-layered hybrid composite with a good elongation at rupture enhanced ductility. This result challenged the widely held hypothesis that FRP strengthened beams were subject to a decline in ductility followed by a brittle and unexpected failure.

AFRP strengthened RC beams made of M25 grade concrete were the subject of an investigation by More and Kulkami [25]. Twenty specimens (100 mm x 150 mm x 1200 mm) in all were tested; two beam specimens served as control beams, while the remaining specimens were tested for varying levels of damage (i.e., 0, 70, 80, 90, and 100%). The findings showed that 1) Compared to the control beam, the ultimate load carrying capacity of beams with 0% damage degree was enhanced by 27.59% and 48.27%, respectively, after reinforcing with a single layer and a double layer of 100 mm wide AFRP strip. 2) As the layer of the AFRP strip was raised, the ultimate load-carrying capability of beams improved. Applying the AFRP strip reduced deflection at the ultimate load as the severity of the damage increased. 4) While 90% and 100% damaged degree beams did not significantly increase their load-carrying capability, 0%, 70%, and 80% damaged degree beams performed better in terms of load-carrying capacity.

The effectiveness of RC beams reinforced with BFRP under quasi-static loading was researched by Chen et al. [26]. The experiment's findings revealed that 1) FRP rupture could replace FRP debonding as the failure mode when used as an anchor system. In

comparison to vertical U-jackets, inclined U-jackets were significantly more effective at using the same quantity of materials. 2) Utilizing U-jackets, the anchorage was able to provide significant anchorage and postpone debonding by boosting the load-carrying capacity of B150A from 20 to 37.8% of B150B. 3) The load-carrying capability of B150D increased from 33.4 to 37.8% of B150B with full coverage of U-jackets anchorages. 4) The load-carrying capability of B150C anchored with inclined U-jackets increased from 37.7% of B150B to 55.2%. 5) The Beam B150B with West System 105-206 adhesive had a little better load-carrying capability, but it was less ductile. This was in contrast to the Beam B330B with SikaDur 330 adhesive.

Using various arrangements of AFRP on RC beams, Raval et al. [27] experimentally investigated the improvement in shear strength. To examine the effects of the arrangement on shear strength, eighteen beams were produced, nine of which were made of M20 Grade concrete and 9 of which were made of M25 Grade concrete. In order to boost the shear strength of RC beams, the study demonstrated that the vertical strip arrangement (48.66% increase in shear strength) outperforms the 45° strip arrangement (36% increase in shear strength).

The effectiveness of BFRP in fortifying reinforced concrete beams was studied by Madotto et al. [28]. A four-point bending load system was used to evaluate seven concrete beams as specimens. Systems for shear and flexural strengthening were made using a variety of unidirectional BFRP fabric qualities. The experimental findings showed that the BFRP fabric successfully boosted the tested beams' shear strength and flexural capacity. The specimens' ductility greatly increased as well.

Using combined externally bonded FRP sheets and near-surface mounted FRP rods, Panahi et al. [29] quantitatively investigated the flexural strengthening efficacy of reinforced concrete beams. The drawbacks of these technologies can be mutually solved by combining EBR and NSM methodologies. Based on a four-point bending numerical simulation, it was determined how varied material qualities, geometrical conditions, and configurations affected the flexural behavior of strengthened beams using the planned procedures. Their research revealed that: 1) NSM-FRP rods considerably increased the flexural capacity and stiffness of reinforced concrete beams as compared to the control beam. The mid-span deflections of reinforced beams during failure, in contrast, primarily decreased as compared to the control beam. 2) With an increase in material strength and embedded length, the ultimate bending moment and stiffness of beams increased. The effectiveness of strengthening approaches on model flexural behavior was proven by

comparing the outcomes of reinforced concrete beams that had undergone strengthening to those of a control beam. 3) The load-deflection behavior of all reinforced specimens made of FRP composites generally followed the same pattern, exhibiting an almost tri-linear response characterized by concrete cracking, steel yielding, and post-yielding stages leading to the failure mode. The first stage of the reinforced beams' behavior before cracking was characterized by linear elastic behavior. At this point, the deflection and concrete cracking moments were affected by the FRP composites. After this step, FRP sheets' reinforcing strength was used. Compared to the control beam, the beams gradually gained stiffness and load-bearing capacity all the way to the ultimate bending moment. By adding more loads, the beam's mid-span deflection rises more quickly than in the earlier phases. 4) With an increase in FRP sheet width, reinforced concrete beams strengthened with EB-FRP sheets were able to handle more weight. Although the bigger FRP sheet on the beam made it less flexible than the narrower FRP sheet. 5) The ultimate bending moments of the reinforced beams were roughly 3.28–5.56 times greater than those of the control beam. As a result, the EBR approach proved effective in strengthening reinforced concrete members' flexural integrity. For beams with b = 40, 80, 100, 120, and 150 mm, respectively, the ultimate bending moments rose by 20, 49, 54, 58, and 69% as compared to the model with an FRP sheet width of 20 mm. 6) A strengthened reinforced concrete beam's bending moment at the mid-span rose with an increase in FRP sheet thickness, according to a finite element simulation of the reinforced concrete beams. The ductility and deflection at the failure of strengthened reinforced concrete beams increased as the FRP thickness increased, in contrast. The ultimate bending moments of specimens with FRP sheets rose by 20, 75, and 116% in comparison to the beam with t = 0.1mm for t = 0.2, 0.5, and 1 mm thicknesses, respectively.

The FRP sheet bonding method has a very clear result, it may be said. However, the primary drawbacks of the EBR technique's performance are the high likelihood of a brittle failure mode, which is primarily brought on by premature debonding of FRP sheets from the concrete substrate, and the susceptibility of FRP materials to environmental factors. A slight delay in the debonding phenomenon can be achieved by providing adequate end anchorages at the ends of the plates and at crucial points along the span, such as U, L, and X-shaped wrappings, as well as by using different surface preparation techniques, like sandblasting, water jet, and air-jet surface roughening.

An experimental program was carried out by Jumaat and Alam [30] to assess the structural behavior of CFRP laminate flexurally enhanced reinforced concrete beams and

anchored steel plate beams. Five beams in all, measuring a combined 2300 mm in length, 125 mm in width, and 250 mm in depth, were created and put to the test. Two beams received steel plate reinforcement, two other beams received CFRP laminate reinforcement, and one beam, the control beam, was left un-strengthened. In order to prevent early failure, one of each of the reinforced beams made of the steel plate and CFRP laminate was left unanchored, while the other was anchored by L-shaped plates at the end and the shear spans (intermediate anchored). Overall, the findings of their experiments demonstrated that the strengthened beams had better failure modes and higher failure loads than the control beam. Results also showed that, in comparison to unanchored strengthened beams, the ends with intermediate anchored strengthened beams produced larger failure loads and better failure modes.

Godat et al. [31] proposed several anchorage methods, including NSM, FRP extension, FRP insertion, horizontal FRP, FRP patch, FRP rope, FRP spike, metallic anchors, and combined anchors, to prevent or delay the debonding failure mechanism and to enhance and recover the ability of externally bonded (EB) fiber-reinforced polymers (FRPs) shear-strengthened beams. Their research is a state-of-the-art analysis of experimental tests that looked into how well anchorage methods for FRP shear-strengthened beams worked. Based on the factors that have a substantial impact on how FRP shear-strengthened beams behave, the various anchorage systems were assessed in terms of FRP shear strength and FRP strain.

Additionally, new procedures known as the EBROG and EBRIG methods were suggested in order to increase the load-bearing capacity of RC members and delay or completely remove the debonding of FRP sheets in strengthened beams employing EBR techniques.

Externally Bonded Reinforcement On Grooves (EBROG) was developed by Mostofinejad and Shameli [32] to delay or prevent the debonding of FRP sheets from the concrete surface in concrete beams strengthened for flexure. Their research showed that the EBROG approach significantly reduced, and in some cases completely eliminated, debonding when sheets were bonded to the concrete substrate. Their research intends to evaluate the effectiveness of the grooving technique when applied beneath multilayer FRP sheets. With standard surface preparation and the EBROG process using various layers of FRP composite, beam specimens with dimensions of 120 x 140 x 1000 mm (width x height x length) were cast and reinforced. The strengthened beams were then put under four-point flexural loading. The outcomes demonstrated that the EBROG method offers

larger failure loads in the beams reinforced with several FRP layers than conventional surface preparation.

Another Externally Bonded Reinforcement In Grooves (EBRIG) method was created by Mostofinejad and Shameli [33]. Thirty-two beam specimens measuring 120 x 140 x 1000 mm were cast, strengthened with one, two, or three layers of FRP sheets, and then put to four-point flexural pressure. The results showed that beams strengthened using the EBROG and EBRIG techniques had much higher ultimate limits than beams strengthened using the EBR approach. When using multiple-layer FRP sheets, the EBRIG approach performed as well as the EBROG method for failure loads and displacements.

To create alternatives to conventional surface preparation techniques, Mostofinejad and Mahmoudabadi [34] looked into surface preparation for applying FRP sheets. For this study, four-point flexural loading was applied to at least 100 prism specimens with dimensions of 100 x 100 x 500 mm. The samples were split into two groups: control and experimental. Transverse, longitudinal, and diagonal grooves were used as a surface preparation replacement while FRP sheets were examined for their ultimate failure strength in the experimental group. The findings demonstrated that prior to bonding, surface pretreatment of FRP sheets increased final rupture strength. It was also shown that the alternative preparation techniques more than made up for the loss of standard surface preparation, in some cases altering the member's eventual failure behavior.

Mostofinejad and Tabatabaei [35] looked into how surface preparation affected the shear reinforcement for RC beams and proposed using the grooving approach in place of traditional surface preparation. thirty-two miniature concrete beams that underwent a four-point loading test served as the experimental specimens. Their research demonstrated that, while surface treatment of concrete prior to connecting the FRP sheets does not always prevent debonding, it can greatly delay debonding and raise beam carrying weights by up to 12%. The outcomes also showed that the grooving technique outperforms surface preparation. All of the beam specimens strengthened with this technique did not have FRP strip detachment, and beam shear weakness was eradicated. The most prevalent type of failure is now a flexural failure.

In order to establish sufficient bonding between CFRP sheets and the concrete substrate, Mostofinejad et al. [36] investigate the impact of the EBRIG and EBR methods for shear strengthening structural components when combined with different CFRP sheet installation procedures. Seven concrete beams (120 x 160 x 1400 mm) were cast, and the four-point loading method was used to evaluate them. Each specimen underwent two tests

totaling 14 tests because external shear anchorages were provided for each span of the beams independently. One specimen served as the control beam while the other six were strengthened utilizing the EBR or EBRIG techniques. According to the experimental findings, the EBRIG and EBR techniques in combination with the full wrapping approach increased load-carrying capacity by roughly 148% and 141%, respectively, compared to the control specimen without CFRP strengthening. The failure mechanism was also seen to alter from a brittle shear failure when using the EBR approach to the preferred flexural mode when utilizing the EBRIG method, which is a noteworthy outcome.

2.4.2 Studies and applications of FRP materials for strengthening/repairing RC members under impact loading (single loading method)

Rockfall, car collisions, ship impacts, and unintentional object drops on structures are just a few of the impact loads that RC structures may experience during their service life. In order to reinforce RC members against impact loading as well as static loading, FRP materials may be employed. The usual studies and applications on FRP materials used to reinforce RC beams subjected to impact loads are listed below.

The impact resistance of RC beams enhanced by FRP sheet bonding to tension-side surfaces was assessed by Kishi et al. [37]. On beams strengthened by gluing FRP sheets to surfaces on the tension side, testing for low-velocity impact loads were performed. In this work, the material characteristics of AFRP and CFRP sheets were examined to see how they impacted the behavior of RC beams under impact loading. 1) Flexural cracks from the lower concrete cover only appeared near the loading area during static loading; however, during impact loading, flexural cracks appeared from both the lower and higher concrete covers throughout the entire span area, with diagonal cracks appearing directly beneath the loading point. 2) Whether or not the RC beams were reinforced with a FRP sheet, the failure mode of the beams shifted from flexural to flexural-shear when the loading changed from static to impact. The diagonal crack tip's peeling action caused the FRP sheet to split off the beam, which resulted to the strengthened beams failing. 3) No matter whether the specimen was reinforced with a FRP sheet, the affected concretes had the same material characteristics, such as compressive strength, elastic modulus, and mass per unit volume, therefore the time histories of the impact force at the beginning of the collision were comparable. 4) If the two sheets' axial stiffnesses were comparable, then the history of the response force, impact force, and the loading point deflection would be identical under impact loading. 5) Both beams successfully debonded the FRP sheet at a

comparable input impact energy because of the peeling activity at the diagonal crack's tip. 6) Although FRP sheets' flexural strengthening lowers the energy that the beam dissipates, the effect might be minimal. Each reinforced beam's energy properties also changed based on the type of sheet used.

In order to determine the criteria for the failure mode of RC beams reinforced with FRP sheets under impact loading, Kawarai et al. [38] performed falling-weight impact tests on RC beams reinforced with FRP sheets while controlling for the volume of the FRP sheet. These were the findings of this study: The impact-resistant capacity of the beams can be improved (1) by using the AFRP sheet bonding method; however, (2) in the case of compression failure mode statically, the beams reach the ultimate state with sheet rupturing; (3) in the case of sheet debonding failure mode statically, the beams reach the ultimate state with sheet debonding.

Four 8 m beams, two with CFRP laminates and two with steel plates, were evaluated for flexure by Erki and Meier [39]. Impact loading was produced by lifting one end of the simply supported beams and dropping it from specific heights. According to their research, beams that had CFRP laminates externally reinforced performed well under impact stress. They could not, however, absorb as much energy as beams that had steel plate reinforcement on the outside. Increased anchoring would increase the impact resistance of these beams, at least at the extremities of the CFRP laminates. The developed equation of motion produced precise predictions using the flexural stiffness of the beams at their ultimate limit condition.

The impact impacts of fiber-reinforced polymer laminates on concrete beams were examined by Tang and Saadatmanesh [40]. Two varieties of composite laminates, including carbon and Kevlar, were adhered to the upper and lower surfaces of concrete beams using epoxy. Two beams received Kevlar laminate reinforcement, two received carbon laminate reinforcement, and one unmodified beam served as the control specimen. The impact load was applied by dropping a steel cylinder from a specific height onto the top face of the beam. The findings showed that composite laminates greatly improved the concrete beams' ability to withstand impact loads. The laminates also decreased deflection and crack breadth. The strength increase is dependent on the type, thickness, weight, and material qualities of the composite laminate, it was found when the test results of beams reinforced with Kevlar and carbon laminates were compared.

Pham and Hao [41] examined the impact behavior of RC beams strengthened with FRP and the contribution of FRP to shear strength. Tests were performed on thirteen RC

beams (150 x 250 x 1500 mm) under static and impact stresses. To test the efficacy of various wrapping techniques, FRP U-wraps and 45°-angle wraps were used to reinforce the beams. According to the experimental findings, FRP debonding strain is a little bit lower under impact loads than it is under static loads. In terms of load capacity and displacement, 45°-angle FRP wraps outperform FRP U-wraps when utilizing the same quantity of FRP. It was more effective to completely wrap an RC beam with FRP than to use scattered FRP strips.

The behavior of RC beams strengthened with FRP under static and impact stresses was studied by Pham and Hao [42]. Both static and impact loads were tested on six and seven beams, respectively. These beams had reinforcement using longitudinal FRP strips and U-wraps. To lessen the stress concentration of FRP U-wraps and give a confinement effect on longitudinal FRP strips, a curved soffit was added to the section of four beams. Comparatively to equivalently-sized fiber-reinforced polymer-enhanced rectangular equivalents, the experimental findings demonstrated that the proposed alteration greatly boosted the beam capacities. All the tested beams saw a shift in failure mode from flexure failure under static loads to shear-flexure failure mode under impact loads. According to the experimental findings, the impact resistance should be designed using the impact force and inertial force at the very beginning of an impact event.

When reinforced concrete beams are subjected to concentrated impact loads at their mid-span, Cotsovos [43] suggested a straightforward approach for assessing the load-carrying capability of the beams. According to the method, a reduction in the length of the portion of the beam that has been found to resist the action of the applied load under increasing loading rates through both experiment and numerical analysis will result in an increase in load carrying capacity. By comparing the suggested technique's predictions to published experimental data and numerical findings produced from three-dimensional dynamic nonlinear finite-element studies, the proposed method was shown to be valid.

GFRP bars were used as internal reinforcement in a study by Goldston et al. [44] to examine the impact on concrete beam behavior. Investigations were done on the beam's static and dynamic (impact) properties. The design, casting, and testing of twelve GFRP RC beams. Six GFRP RC beams were put to the test with static loads in order to study failure modes and related energy absorption capacities. At the University of Wollongong, the remaining six GFRP RC beams were put to the test using a drop hammer machine. A larger reinforcement ratio resulted in GFRP RC beams with increased post-cracking bending stiffness and flexural-critical failure under static stress. GFRP RC beams under

impact loading, however, failed in a "shear plug" fashion in the impact zone, regardless of their shear capability. It was determined how much energy each beam could absorb. In comparison to static moment capacities, the average dynamic amplification factor was calculated to be 1.15, showing larger dynamic moment capabilities (15–20% increase). The behavior of GFRP RC beams was influenced by the reinforcing ratio and concrete strength.

The dynamics of sheet debonding in an externally reinforced beam were studied by Rabinovitch [45]. The study focused on how dynamics affect debonding behavior and brought out two facets of this interaction. The initial one is the impact of debonding on the development of dynamic responsiveness. The second is how the dynamic structural reaction affects how the debonding process starts, develops, lasts, and is stable. These two features were highlighted by computational analysis of a broken beam that had a composite layer for reinforcement. The dynamic debonding process was characterized numerically in terms of load, displacements, stress resultants, adhesive layer stresses, and interfacial tractions across the cohesive interface over time. Additionally, it tracked the debonding front's motion and speed during the failure process. It examined the impact of the loading rate on the dynamic interfacial process last.

Pham and Hao [4] provide a summary of the impact resistance of FRP-reinforced buildings, including RC beams, slabs, columns, and masonry walls. According to their research, 1) RC structures such as beams, slabs, columns, and masonry walls can have their impact resistance improved by using FRP materials. Increased ductility, load-carrying ability, and energy absorption are the results. 2) Although the tensile strength of FRP materials rises with strain rate, the failure strain and the stress-strain relationship could not be determined. 3) The FRP's rupture strain under impact loads and the method by which it debonds remain a mystery. 4) Reverse loads in RC slabs and beams can produce negative moments, which can result in unanticipated failures. The design needs to take them into account after doing some study.

Using twenty-seven concrete beams, Tang and Saadatmanesh [46] examined the behavior of beams strengthened with FRP laminates under impact loading. Due to their lack of retrofitting, two of the twenty-seven beams were used as control specimens. The impact force was generated by a steel cylinder drop weight. Their research showed that gluing composite laminates to concrete beams could greatly increase the structure's resistance to impact loads. The beams' residual stiffness and cracking and flexural strength were both enhanced by bonding laminates. Additionally, the total number of

cracks, the width of the cracks, and the maximum deflection were all decreased. The maximum deflection was reduced by 30 to 40% and the residual rigidity of the strengthened beam was two to three times larger than that of an un-retrofitted beam after the initial impact. The composite laminate's kind and weight have an impact on the improvement. The final deflection, crack count, and crack breadth were lower in comparison to static test results. The greatest reaction force was, however, three to four times more than the beam's under static loading. One can use a regression equation to calculate the strengthened beam's remaining stiffness after the initial impact. An equation built using Spring-Mass models and adjusted by test results can be used to compute the impact force. Flexural wave theory has been used to derive an equation for forecasting a beam's deflection brought on by impact loads.

To better understand the failure behavior of RC beams under impact load, Zhan et al. [47] carried out a series of high-speed impact experiments using an instrumented drop-weight impact machine. 1) Under static loads, the stiffness of the beam increased as the reinforcement ratio and concrete strength increased; the load-carrying capacity of the beams also increased as these factors grew; and the static maximum deflection of the beams dropped as these factors increased. 2) For a particular mass of drop-weight, there was a particular threshold velocity. Expanding the flexural load capacity of RC beams was no longer possible, and increasing the stress (or strain) rate had no effect on how much load they could support. 3) The scale factors varied greatly depending on whether the drop-weight followed the beam or rebounded, even though the impact impulse was proportional to the momentum of the impacting mass. 4) The maximum and residual deflections for the input impact energy were almost proportional. The gradient could be determined empirically by taking the inverse of the static flexural load-carrying capacity of the beam. 5) On the basis of these relationships, two empirical formulations that take into account the static flexural load-carrying capacity, maximum deflection and/or residual deflection, and input impact energy were developed. Discussions over the applicability of the presented equations involved comparisons with other experimental findings. The outcomes of the two equations were consistent with the additional experimental and analytical data.

The behavior of RC beams reinforced with CFRP laminates was examined by White Timothy W. et al. [48]. Nine 3 m RC beams were tested with four different loading schedules: one without strengthening, four with S-type CFRP laminate reinforcement, and four with R-type laminate reinforcement. 0.0167 mm/s (slow rate of loading) to 36

mm/s (rapid rate of loading) were the different stroke speeds (fast rate of loading). As a result, the CFRP's strain rate increased from 2.96 /s (a sluggish pace) to 6,930 /s (a fast rate). Some beams underwent 1 or 12 cycles of loading prior to a rapid loading rate to failure. 1) Their experimental and analytical tests show that strengthening with CFRP increases flexural capacity and stiffness but decreases energy absorption and ductility. 2) The quantity of CFRP reinforcement, the amount of steel reinforcement, and the failure mode all affect how big these changes are. 3) When compared to identical beams loaded slowly (10^{-6}/s) or rapidly (10^{-3}/s) stressed beams show a 5% increase in flexural capacity, stiffness, and energy absorption. 4) Preloading for 12 cycles has no detrimental effects on the enhanced CFRP beam's ability to flex. 5) The moment-curvature response can be precisely modeled using a layered, finite-element analysis.

Wang [49] examined the flexural response of flax fiber reinforced polymer (FFRP) laminate-wrapped coconut fiber reinforced concrete (CFRC) beams under static and impact loadings. Three alternative fiber contents, namely 1%, 3%, and 5% of cement mass, corresponding to fiber volumes of 0.4, 1.2, and 2%, were taken into consideration. They found that

Static loading tests:

1. With 4.92 MPa and 13 MPa for CFRC and FFRP-CFRC beams, respectively, the flexural strength of FFRP-CFRC beams was almost three times that of CFRC beams.

2. While CFRC specimens functioned as smooth curves, the force-deflection curves of the FFRP-CFRC beams had an almost bi-linear tendency. There were differences between the failure patterns of CFRC and FFRP-CFRC. The CFRC examples were connected by the coconut fiber, which also showed some ductility and prevented cracks from forming right away. However, brittle failure occurred close to the beam center in FFRP-CFRC beams.

3. While enhancing the ductility of the FFRP-CFRC beams, the coconut fiber content had minimal impact on flexural strength.

Impact loading tests:

1. The amount of coconut fiber had an impact on how many blows were necessary to shatter the specimen in the repeated test. The FFRP-CFRC specimens with 1%, 3%, and 5% coconut fiber content required 3, 3, and 2 blows to break, respectively.

2. In comparison to specimens with a 1% and a 5% coconut fiber content, FFRP-CFRC specimens with a 3% coconut fiber content absorbed the maximum energy, or roughly 83.23 J.

3. The strain rate, rather than the amount of coconut fiber used, had an impact on the FFRP-CFRC beams' dynamic increase factors (DIFs) in the single impact test. The DIF value increased with the strain rate. To better explain the connection between strain rate and DIF, an empirical equation was suggested.

In order to forecast how FRP laminates would react and fail when subjected to impact loadings, Liu et al. [50] carried out a numerical analysis with an emphasis on delamination. 1) In numerical simulations of the reaction and failure (delamination) of FRP laminates subjected to impact loadings, the cohesive interface layer's strain rate effects must be taken into account, according to their research. 2) Controlling impact-induced delamination of FRP laminates requires strong cohesive interface layers; the smaller the delamination area, the stronger the cohesive interface layer.

The effects of the sheet volume and input impact energy on the failure modes of strengthened RC beams were examined by Sinh et al. [51]. The RC beams enhanced with AFRP sheets underwent drop-weight impact loading testing. Investigated was the sheet volume, which ranged from 415 to 1660 g/m^2. The impact force was produced by dropping a 300 kg steel weight from various heights (0.5, 1.0, 2.0, 2.5, 3.0, and 3.5 m) into the midspan of the beams, and the weight's drop height was increased until the sheets were debonded or ruptured. Non-strengthened beams were also assessed as reference beams. The results of this study are as follows. 1) By using the AFRP sheet bonding method, it is possible to increase the impact resistance capacity of strengthened beams by up to 85% in the event of impact loading; however, 2) in the event of relatively high impact energy, the impact resistance capacity may not always be remarkable. 3) The failure mechanisms of the AFRP-strengthened beams were divided into two categories based on the sheet volume: sheet debonding and sheet rupturing. The debonding of the AFRP sheet of the strengthened beams may not be improved by 4) increasing the sheet volume.

2.4.3 Applications of FRP materials for strengthening/repairing RC members under consecutive impact loading

Actually, the structure is frequently subjected to a series of impacts with escalating impact energy. In order to strengthen the RC construction, FRP materials have also been utilized. Below is a list of some typical studies on this subject.

In order to develop a practical approach for increasing the impact-resistant capacities of the RC beams employing FRP sheets, Kishi et al. [52] experimentally studied

the beams strengthened in flexure with AFRP sheets under sequential drop-weight impact loading. A 300 kg steel weight was dropped from a predetermined height under impact, and the height was gradually increased by 1, 2, and 3 m to attain the ultimate state of the beam. The findings of their investigation suggested that 1) the sheet's strengthening effects under impact loading may be more than twice as great as those under static loading. 2) It is reasonable to assume that strengthened RC beams with an AFRP sheet will have an impact energy accumulation that is more than double that of unenhanced RC beams.

To develop a rational technique for enhancing the impact-resistant capacities of the RC beams employing FRP sheets, Le Huy et al. [53] experimentally studied the beams strengthened in flexure with AFRP sheets under sequential drop-weight impact loading. In this work, the tension-side surface of the beams was bonded to the AFRP sheet, which has a density of 1660 g/m^2. These RC beams have a rectangular cross-section with dimensions of 200 mm in width, 250 mm in depth, and 3 m for the clear span. A 300 kg steel weight was successively dropped into the beam's mid-span from a predetermined height to apply the impact load. To reach the matching final state of the beam, the height was increased in increments of 1, 2, 2.5, and 3 m. The experimental outcomes demonstrated that 1) AFRP sheet reinforcement effectively reduced maximum and residual deflections. 2) A cumulative input impact energy was represented by a linear distribution of the absolute maximum and residual deflections. 3) With the sheet debonding, the RC beams that had been strengthened with the AFRP sheet attained their final state.

To examine the impact responses of CFRP-reinforced RC beams, Fujikake et al. [54] carried out an experimental investigation. The experiment examined the effects of drop height, the number of strikes, and the CFRP strengthening scheme on its reaction. It employed a drop hammer impact test. Four distinct CFRP strengthening techniques were used to reinforce RC beams. According to their experimental study, 1) the fracture width of RC beams in flexure that had been strengthened with CFRP was less than 10% smaller than that of RC beams that had not been strengthened. 2) End anchorages are inserted at both ends of the CFRP sheets attached to the soffit of the RC beams to help prevent the soffit CFRP sheets from debonding, allowing the CFRP strengthened RC beams with end anchorages to bear reasonably high impact loads. 3) End anchorages with anchor bolts and steel cover plates were very effective for strengthening RC beams with pultruded CFRP laminates against rather substantial impact loads. 4) RC beams can endure twice

the drop height necessary to trigger the failure of unreinforced RC beams when sufficiently strengthened with CFRP.

2.5 Summary

This chapter covers two widely utilized reinforcement techniques: FRP sheet bonding and FRP rod near-surface installation (NSM). The benefits and drawbacks of each strategy have been looked at. The sheet bonding technique (EBR technique) is quick and simple to install and has low ongoing costs. If the bonding between the FRP sheet and the concrete substrate is not under control, premature FRP sheet debonding has a drawback. The FRP rod near-surface mounted approach is a cutting-edge method. With this method, performance is increased, early failure is decreased, and protection from fire, mechanical harm, aging, and malicious acts is increased. However, trenching pollutes the environment and is not always feasible. The EBR approach was used for this investigation because it installs swiftly and simply. The mechanical attributes of FRP materials were also covered in this chapter. CFRP, GFRP, AFRP, and BFRP fibers are examples of typical FRP materials. These materials are used to strengthen constructions that are susceptible to both static and dynamic loads. To comprehend the practical effectiveness of externally bonded FRP systems for strengthening concrete structures, typical research and applications of FRP materials have been detailed.

Chapter 3: EXPERIMENTAL OVERVIEW

3.1 Introduction

The experimental methods and sample types employed in this study are outlined in this chapter. Additionally, the loading technique, measurement items, and attributes of the used materials (concrete, steel reinforcement, and FRP sheet) are explained. The measurement tools utilized in this experiment will also be described.

3.2 Specimen outline

A total of twenty-five RC beams were examined in this study, comprising four unreinforced beams and twenty-one beams that had their flexure strengthened utilizing the AFRP sheet bonding technique.

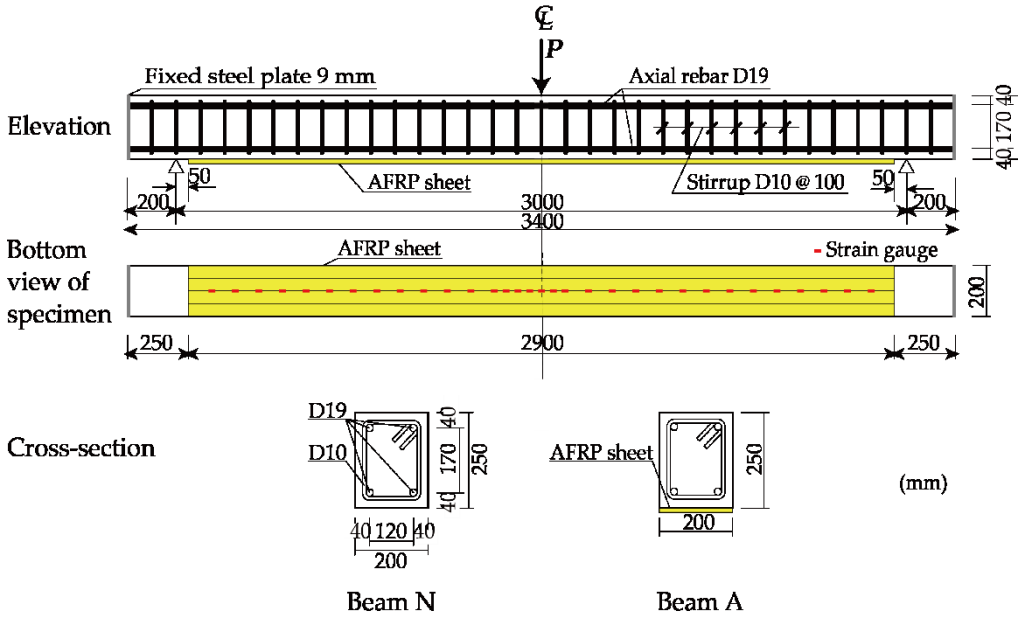

Figure 3.1. AFRP sheets and rebars' sample dimensions and arrangements [51].

Figure 3.1 displays the specimen's measurements as well as the arrangement of the rebars and AFRP sheets. The cross-sections of the beams, which were all rectangular and had dimensions of 200 mm broad, 250 mm deep, and 3 m long (clear span), were chosen to suit the laboratory environment and the test apparatus.

At the edges of the beams, 9-mm-thick steel plates were welded to 19-mm-diameter axial rebars to make sure they were fully anchored and to shorten the spacing between the support point and the free edge. This made the part have less of an effect on how the beam responded to an impact. Here, two rebars were positioned on the upper side and two rebars

on the bottom side. Furthermore, stirrups with 10 mm diameters were spaced 100 mm apart. The beams were cast using ready-mixed concrete and the mix proportions from the table in Table 3.1. Figure 3.2 depicts the casting process for RC beams. With 50 mm between each sheet's end and the support point, the AFRP sheets were attached to the tension-side surfaces of the beams. To increase its ability to bond, the bonded concrete surface was grit-blasted to a depth of around 1 mm. Following acetone cleaning, primer was applied to the surface.

Table 3.1. Table of concrete mix proportions [51]

W/C (%)	S/a (%)	Unit weight (kg/m^3)				
		Water W	Cement C	Fine aggregate S	Coarse aggregate G	Admixture Ad
52.4	43.0	154	294	812	1064	2.940

(a) Formwork and reinforcement

(b) Concrete casting

(c) Concrete curing work

Figure 3.2. RC beam casting method [51].

The specimens were split up into various experimental groups depending on the study's objectives:

Drop-weight impact loading tests on RC beams reinforced with AFRP sheets were performed in order to examine impact-resistant behavior, including the strengthening effect and failure modes of the RC beams reinforced in flexure with AFRP sheets. A range of sheet volumes, ranging from 415 to 1660 g/m^2, were used to evaluate how the sheet volume affects the beams' failure mechanism. The 300 kg steel weight was dropped onto the midspan of the beams at a predetermined height to provide the impact force, and the weight's drop height was increased until the sheets separated or ruptured.

RC beams that had been strengthened in flexure with externally bonded AFRP sheets were also put through a series of drop-weight impact loading tests to further examine the RC members' characteristics for resistance to impacts. In order to assess how well beams strengthen structures, the sheet volume and cumulative input impact energy were looked at. 415, 830, and 1660 g/m^2 sheets per meter were used. Up to the matching ultimate state of the beam, the weight's drop height was increased in steps of 1, 2, 2.5, and 3 m. Additionally tested were unreinforced beams for comparison.

The load-bearing capacity, strain distribution, crack distribution, and failure behavior of the beams were instead studied using static loading experiments. The results of these studies were compared to impact loading tests, calculated results, and the previous study's findings to verify the criteria of failure mode of strengthened beams.

3.3 Material properties

According to our earlier research [37], the impact resistance behaviors of the strengthened beams with both FRP sheets were equivalent if the axial stiffness values of AFRP and CFRP sheets were the same. The AFRP sheet was chosen for this study because of its adaptability and simplicity of installation.

Epoxy resin, whose material characteristics are reported in Table 3.2, is the adhesive in this investigation employed to attach the sheet to the concrete substrate. For at least seven days, the epoxy resin was allowed to cure in an environment with temperatures above 200 C and humidity levels below 70%.

Table 3.2. Epoxy resin material characteristics [51].

Bending strength (MPa)	Compressive strength (MPa)	Tensile shear strength (MPa)	Adhesive strength (MPa)
40	35	10	1.5

Each beam was strengthened by bonding either a single AFRP sheet that had an areal weight of 415 or 830 g/m^2 or a pair of AFRP sheets that had a combined weight of 1660 g/m^2, with each ply having an areal weight of 830 g/m^2. Figure 3.3 provided an overview of the AFRP sheet bonding process.

(a) Surface treatment

(b) Epoxy resin application

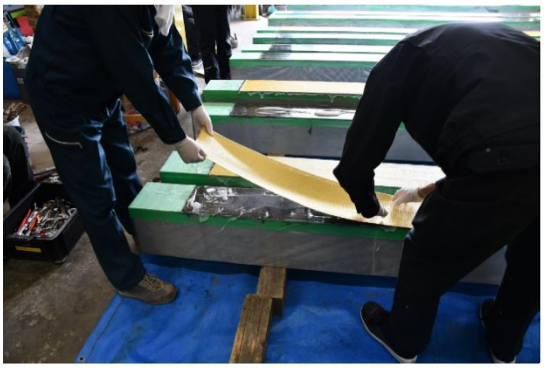

(c) AFRP sheet bonding

(d) Completion and curing

Figure 3.3. AFRP sheet bonding method [51].

Table 3.3. AFRP sheets' material characteristics [51].

Mass per unit area (g/m^2)	Thickness (mm)	Tensile strength (GPa)	Elastic modulus E_f (Gpa)	Failure strain ε_{fu} (%)
415	0.286	2.06	118	1.75
830	0.572			

The manufacturer Fibex [55] provided Table 3.3 with a list of the material characteristics of the AFRP sheets utilized in this investigation. These characteristics were established through testing based on JIS K 7165 [56].

In this experiment, stirrups with a diameter of 10 mm and axial rebars with a diameter of 19 mm had yield strengths of 382/371/394 MPa and 462/402/373 MPa, respectively.

Concrete that was pre-mixed and had a nominal strength of 24 MPa, a slump of 120 mm, a maximum aggregate size of 25 mm, and a 4.5% air content was used to create the RC beams. Table 3.1 presents the mixed proportion table. Concrete has compressive strengths of 32.4, 33.7, and 34.3 MPa.

3.4 Loading test methods

3.4.1 Static loading method

As shown in Figure 3.4, static loading tests were performed using the three-point loading test method. The load was surcharged at the midspan of the beam using a loading jig with a width of 100 mm in the span direction and a hydraulic jack with a 500 kN capacity.

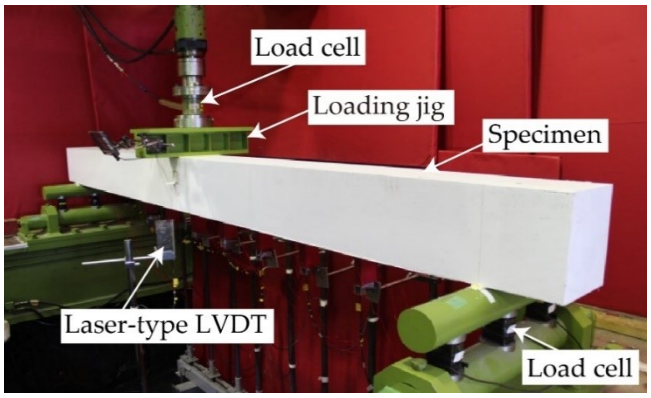

Figure 3.4. View of static loading test setup [51].

3.4.2 Impact loading method

In Figure 3.5, the setup for the drop-weight impact loading test is depicted. To provide an impact load, a 300 kg steel weight was dropped into the midspans of the beams from a predetermined height. The weight was made of a solid steel cylinder that measured 1.4 meters in length and 200 millimeters in diameter at the striking portion, and the impact surface has a 2-millimeter taper to prevent one-sided contact.

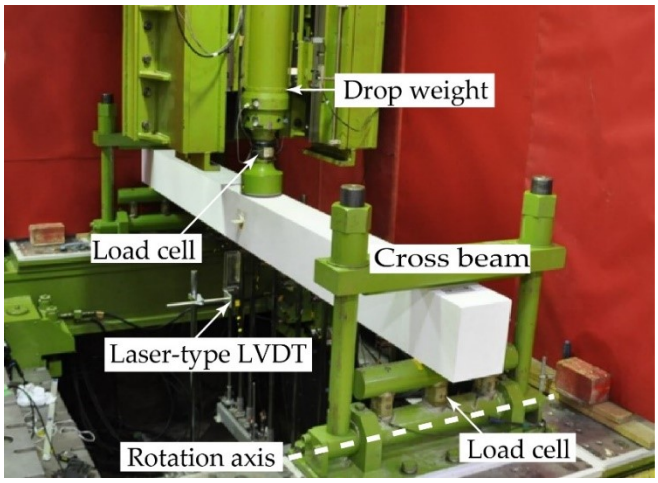

Figure 3.5. View of drop-weight impact loading test setup [51].

3.5 Measurement system

During this experiment, the impact force *P*, the total response force *R*, the midspan displacement (thus displacement) *D*, and the axial strain distribution of the AFRP sheets were all recorded. Measurement of beam deflections, including residual deflections after impact loading, was done using linear variable displacement transducers of the laser type. The dynamic behavior of the beams close to the loading point was observed using a 2,000 fps high-speed camera. A sketch of the crack patterns on one side of the beam was drawn after each test.

Analog signals from the sensors were amplified and recorded using digital data recorders for both experiments. This analog data was transformed into digital data at intervals of 0.1 seconds for the static loading tests and 0.1 milliseconds (ms) for the impact loading tests. In this study, the moving rectangular average approach with a 0.5-ms window was used to numerically smooth the time histories of the response force *R* and deflection *D* for the impact loading experiments.

Chapter 4: STATIC BEHAVIOR AND FAILURE MODE OF STRENGTHENED RC BEAMS

4.1 Introduction

The conventional techniques for bolstering or modifying existing concrete structures include steel plate bonding, section expansion, and external post-tensioning. These methods, however, have drawbacks, including weight increase, installation challenges, and corrosion of the reinforcing material, which raises maintenance expenses. A high strength-to-weight ratio, corrosion resistance, and ease of installation are just a few advantages that FRP materials offer. FRP materials have been the subject of several studies and applications in civil engineering because of these qualities. The use of FRP materials was made to reinforce RC beams in flexure and/or shear under static loads [23–29]. There exist design guidelines for using externally bonded FRP systems to reinforce concrete structures, and these guidelines are frequently used [1]. For the purpose of strengthening the RC structure, externally bonded FRP sheets and near-surface mounted FRP bars are used. The externally bonded reinforcement in grooves (EBRIG) and externally bonded reinforcement on grooves (EBROG) techniques that Davood Mostofinejad et al. suggested are new strengthening methods based on EBR techniques. In addition to increasing the load-bearing capability of RC members, these procedures, as opposed to EBR techniques, can delay the debonding of FRP sheets in strengthened beams [32–36].

The effect of FRP volume on the rupture/debonding of FRP sheets in the strengthened beams has not yet been researched, despite the fact that the flexural load-carrying capacity and failure behavior of reinforced RC beams under static loading have been examined. While M_y and M_u stand for the yielding bending moment at rebar and the maximum moment capacity of reinforced RC beams, respectively, Kishi et al. [21] found that the failure mode of flexural strengthened RC beams under static loading depends on the predicted bending moment capacity ratio M_y/M_u. When M_y/M_u was higher than 0.70, flexural compression failure, which occurs when RC beams fail as a result of sheet debonding after reaching a predicted ultimate compressive state was experienced. Debonding failure was also attained when M_y/M_u was less than 0.65. This is the point at which RC beams fail as a result of sheet debonding prior to reaching a predicted ultimate compressive condition.

To investigate the load-carrying capacity, strain distribution, crack distribution, and failure behavior of the beams from this perspective, static loading experiments were carried out in this chapter. The results of these experiments were compared to impact loading tests, analytical results, and the previous study's findings to confirm the criteria for the failure mode of strengthened beams.

4.2 Experimental method

The samples used in this chapter are shown in Table 4.1. The nominal names of the specimens are included in this table with a hyphen next to the loading type and strengthening material (N: none, A: AFRP) (S: static loading). This table lists the yield strengths of the main rebar, the stirrup, and the concrete's compressive strength.

Table 4.1. List of specimens [51].

Specimen	Compressive strength of concrete $f_c^{'}$ (MPa)	Yield strength of main rebar f_y (MPa)	Yield strength of stirrup f_{sy} (MPa)	Calculated flexural load capacity P_{usc} (kN)	Calculated shear load capacity V_{usc} (kN)	Shear Flexural capacity ratio α
N-S	32.4	382	462	55.0	329	5.98
A415-S	33.7	371	402	81.0	299	3.69
A830-S				99.9		2.99
A1660-S				126.1		2.37

According to the Standard Specification for Concrete Structure [57,58], the predicted flexural and shear load capacity of the beams was determined using the material parameters of concrete, rebar, and AFRP sheets (Table 3.3). The calculations in the reference [57, 58] were used to evaluate the shear load capacity in this instance. The flexural load capacity is determined by computing the maximum load value using the load-displacement relationship curves for each beam. In this chapter, the load-displacement curve's calculating process will be covered. According to Table 4.1, the shear-flexural capacity ratio $\alpha = V_{usc}/P_{usc}$ of all RC beams with/without strengthening is greater than 1.0, which indicates that the strengthened RC beams should statically reach the flexure failure mode.

As shown in Figure 3.4, three-point loading tests were used to conduct static loading tests. The load was applied to Beam A-S, which was reinforced with an AFRP sheet, up

until the point at which the sheet ruptured or debonded. The load was applied until the beam deflected to around 90 mm for Beam N-S, which was not reinforced with an AFRP sheet. This is because the rebar's plastic hardening action caused the load to gradually increase after it yielded.

4.3 Experimental results and discussions for static loading tests

4.3.1 Static load-deflection relationship curve

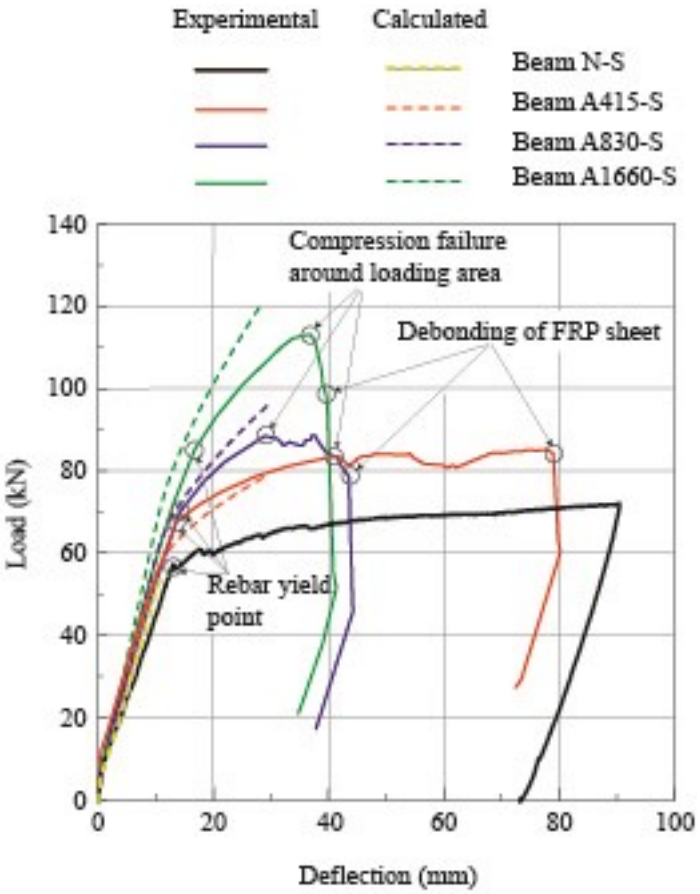

Figure 4.1. Comparing load-displacement relationships of beams in static loading tests [51].

Figure 4.1 compares the static load-deflection curves for the estimated and experimental data for Beams N-S and A-S. While calculated values are represented by dashed lines, experimental data are represented by solid lines. The load-deflection curve and axial strain distribution of the AFRP sheets in this chapter were calculated using the multilayered approach [59], based on traditional material strength methodologies. The following approaches and presumptions were employed: 1) Excellent bonding and a plane

section were required for the concrete and reinforcement, including the FRP sheet. 2) The smeared crack method and the layered strategy were applied. 3) Based on the Standard Specification for Concrete Structure in Japan [57, 58], the stress-strain relationship was assumed for each material, as shown in Figure 4.2. 4) A continuous stress-strain relationship between each layer was presumed.

By segmenting a cross-section of the beam into horizontal layers with 5-mm thicknesses corresponding to either concrete or reinforcements, as illustrated in Figure 4.3, it was possible to properly determine the relationship between the curve and bending moment at each strain level. The thickness of every layer was determined using the pre-analysis data. The neutral axis and lower fiber strain matching to any upper fiber strain of the cross-section were derived by gradually altering the lower strain and taking the resulting force equilibrium of all layers. With the help of these upper and lower fiber stresses, it is possible to determine the related curvature and sectional bending moment. By applying the procedures outlined above from zero to the final state (ε_{cu} = 0.35%), it is possible to determine the top fiber compressive strain of the concrete for these relationships. Due to this, the beam's distribution throughout the span's curves for each loading step matched the diagram of the bending moment. The midspan displacement of the simply supported beam due to curve distribution was ultimately determined using Mohr's integral approach.

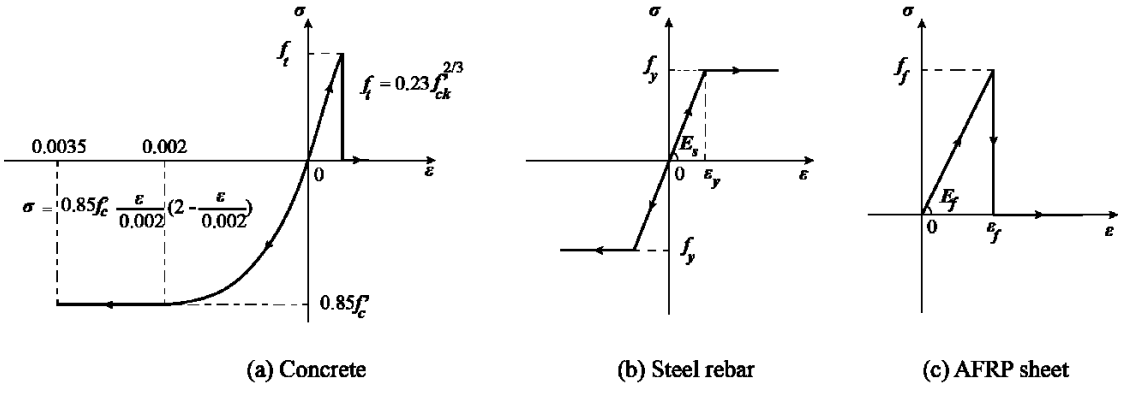

Figure 4.2. Stress-strain relationship for each material [51].

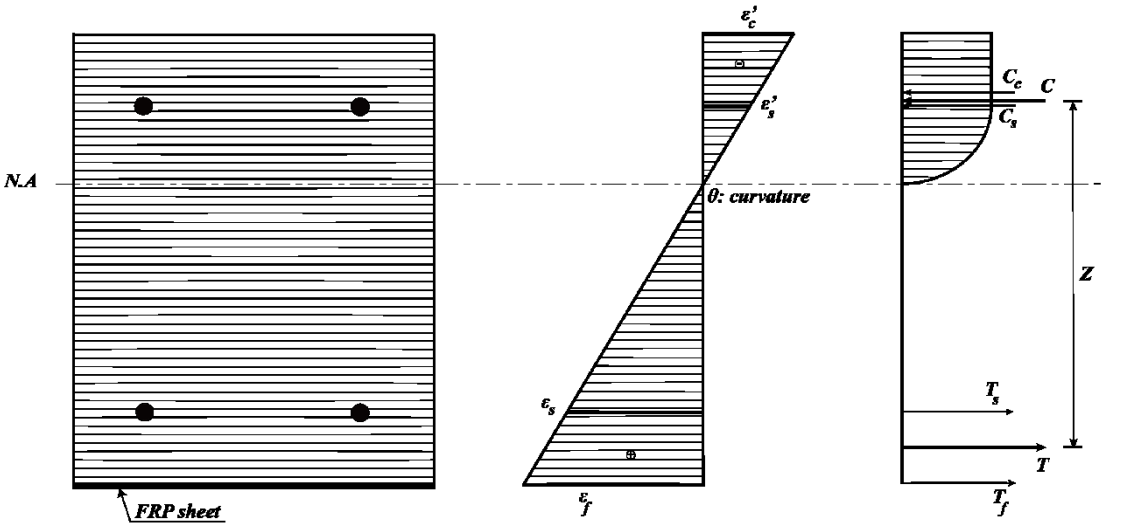

Figure 4.3. Estimation of load-displacement curve [51].

Table 4.2. Calculated and experimental data for static tests of beams [51].

	Specimen	Rebar yield load P_y (kN)		Maximum load P_u (kN)	
		Experimental	Calculated	Experimental	Calculated
1	N-S	57.0	53.3	66.7	55.0
2	A415-S	67.8	57.9	84.8	81.0
3	A830-S	71.5	62.5	88.8	99.9
4	A1660-S	85.5	69.9	112.7	126.1

The experimental and predicted data for Beams N-S, A415-S, A830-S, and A1660-S are presented in Table 4.2 at the main rebar yield and maximum load. Using the second turning point of each load-deflection relationship curve depicted in Figure 4.1, the yielding load was identified in this situation. Since the load grew monotonically because of the rebar's plastic hardening effect, the maximum load for Beam N-S was calculated using the midspan deflection at 40 mm. According to the experimental findings, Beams A–S had yielding loads and maximum loads that were 1.2–1.5 and 1.3–1.7 times higher than those of Beams N–S, respectively. According to the calculated results, Beam N-S reached the ultimate state as soon as the rebar gave way because the upper fiber strain had reached the ultimate compressive state with a value of ε_{cu}= 0.35%, whereas Beam A-S reached the ultimate state due to the sheet debonding failure mode over the predicted deflection at the ultimate state.

Comparing the experimental and calculated findings for Beam A415-S in Figure 4.1 reveals that, up until the beam reached the calculated ultimate state, the calculated result and experimental result were substantially equivalent. The FRP material was thought to entirely adhere to the concrete. The load did not diminish in the experiment even after the calculated deflection was reached at the final condition, indicating that the AFRP sheet's strengthening effect considerably increased the beam's ability to carry loads. As the AFRP sheet debonded at a displacement of about 80 mm following compressive failure in the stress area, Beam A415-S failed.

The measured maximum load for Beams A830-S and A1660-S is lower than the estimated maximum load (Table 4.2). It was proven that the sheet was gradually released from the beams A830-S and A1660-S after the rebar surrendered and/or before the rebar yielded, respectively (Figure 4.1). The lower concrete cover of the beam in the loading area developed crucial diagonal cracks that caused the sheet to peel off, which caused the debonding in this instance. The sheets, therefore, tend to debond earlier than anticipated when the amount of FRP sheets is rather considerable.

These experimental results' failure modes seem to follow the same pattern as earlier studies [21]. Beam A415-S experienced "Flexural compression failure," where it reached its worst condition as a result of the sheet's debonding when the upper concrete cover was broken. The "Debonding failure" category was applied to Beams A830-S and A1660-S because they achieved their ultimate state as a result of the sheet debonding without upper concrete crushing.

4.3.2 Strain distribution of AFRP sheets

For Beams A415/830/1660-S at the predicted ultimate state, which corresponds to the calculated deflection at the ultimate state, Figure 4.4 compares the axial strain distributions computed and experimentally obtained for the AFRP sheet. The anticipated results were based on the multilayered technique [59], as previously described, and assumed complete adhesion between the AFRP sheet and concrete. The center triangle area, which includes the loading point, was found to correlate to the primary rebar yield area based on the estimated results. Due to the rebars' tendency to give at this point, the slope of the strain distribution curve at each half-span of the beam sharply increased at a distance of about 500 mm (the triangular area including the loading point). Along with the rise in the bending moment, the strain distribution linearly grew closer to the midspan point.

According to the figure, although the experimental strain distribution in the instance of Beam A415-S had a few places that were higher than the calculated ones, those roughly better corresponded from the loading point to both ends of the support points to each other. It can be proven that the AFRP sheet and concrete were flawlessly attached to one another up until they reached the predicted ultimate state.

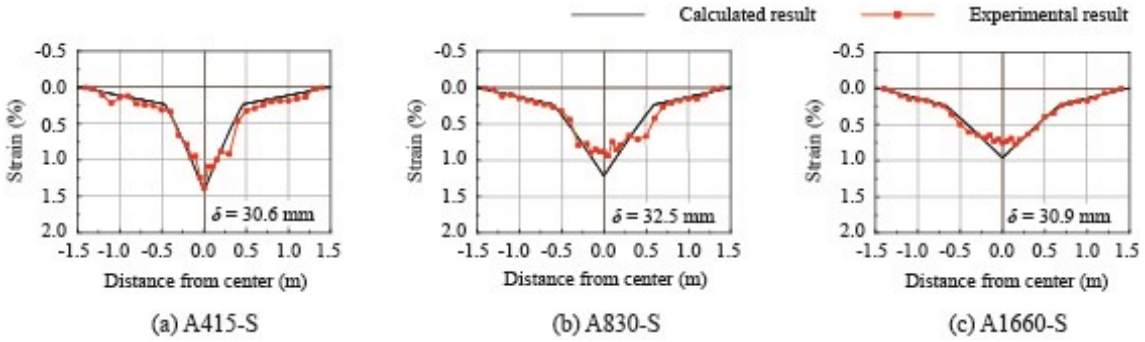

Figure 4.4. Comparisons between calculated and experimental data regarding the AFRP sheet's axial strain distribution at computed ultimate state [51].

The experimental strain distributions for Beams A830/A1660-S were roughly uniform, 500 mm from the loading point, and the experimental strains were lower than the estimated ones, suggesting a tendency for sheet debonding. In addition, it was determined that partial debonding of the sheet had taken place despite the fact that the experimental strain findings were somewhat bigger than the calculated results in the primary rebar yield area.

The figure shows that the strengthened RC beams' AFRP sheet did not tear since the maximum strain did not exceed 1.75% (ultimate strain). It suggests that all of the reinforced RC beams achieved their final state by sheet debonding.

4.3.3 Crack patterns for beams after static loading tests

The fracture patterns of Beams N-S and Am-S following the static loading tests are shown in comparison in Figure 4.5 (m: index of mass per areal unit of FRP sheet bonded for each beam, m = 415, 830, and 1660). Flexural cracks developed from the bottom concrete cover surrounding the loading point in the direction of the loading point for all beams, as depicted in the figure.

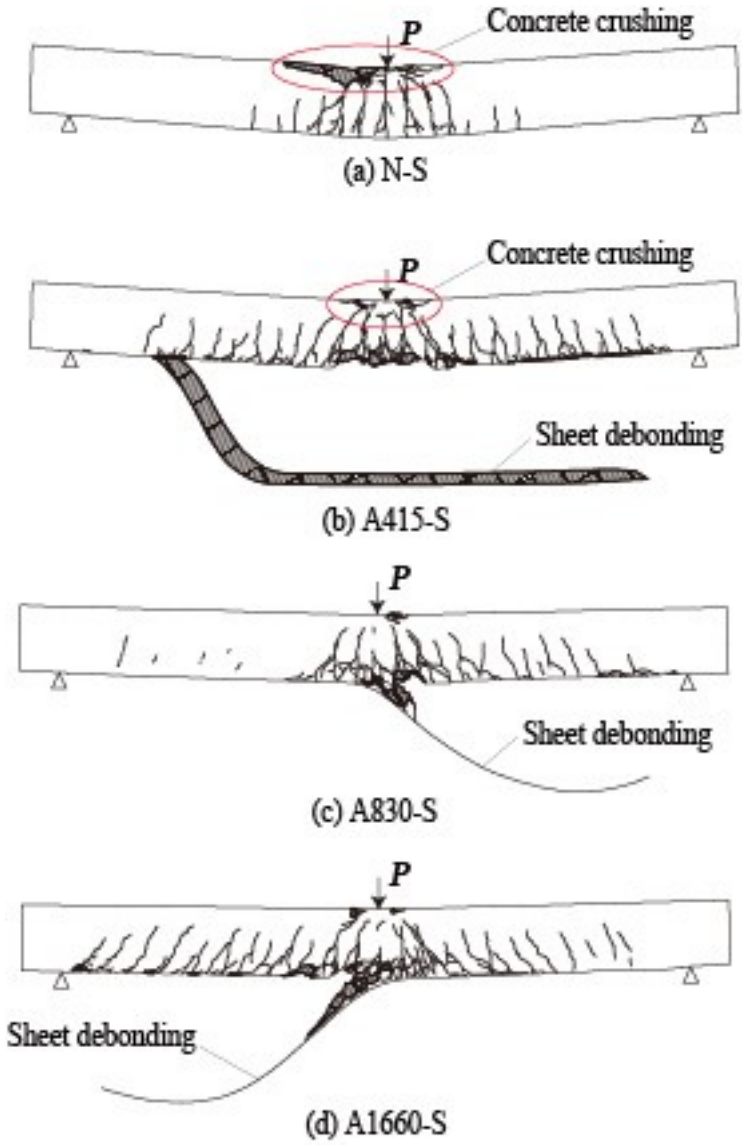

Figure 4.5. Beam crack distribution following tests with static loads [51].

Around the loading area, Beam N-S experienced multiple flexural cracks, extensive damage to the upper concrete cover close to the loading point, and permanent deformation of the beam. With flexural failure mode, beam N-S failed. Due to the strengthening effect of the AFRP sheets, Beam A*m*-S had flexural cracks that were more evenly distributed across the beam than Beam N-S, and the beams were not irreversibly damaged. The higher concrete cover was crushed around the loading point, however, severely damaging Beam A415-S, a strengthened beam. The upper concrete cover of Beams A830/1660-S was damaged, but less so than Beam A415-S. It was not crushed around the loading area. Being less distorted than Beam A1660-S, Beam A830-S had flexural cracks that were most visible on its right side. It might be because Beam A1660-S's sheet was more thoroughly debonded than Beam A830-S's. The lower concrete cover of the beam at the

loading region had critical diagonal fissures that were created by the tips peeling off, which caused the sheet to become unbonded. The sheet debonding with flexural failure mode caused all the reinforced beams to collapse.

The bonding strength between the sheet and concrete may have been more important than the concrete's tensile strength as a result of the sheets debonding from the lower concrete coverings around the loading point (Figure 4.6).

(a) A415-S (b) A830-S (c) A1660-S

Figure 4.6. Photograph of debonded sheet close-up with concrete used for beams [51].

4.3.4 Comparison of failure mode of experimental results with previous study results

Table 4.3. A list of each flexure-reinforced beam's failure mechanisms.

Specimen	P_y (kN)	P_u (kN)	$\frac{P_y}{P_u}\left(=\frac{M_y}{M_u}\right)$	Failure mode
A415-S	57.9	81.0	0.71 (>0.7)	Flexural compression failure
A830-S	62.5	99.9	0.62 (<0.65)	Debonding failure
A1660-S	69.9	126.1	0.55 (<0.65)	

Yield and maximum load are determined in Table 4.3 as P_y and P_u, respectively. This table demonstrates that depending on the computed bending moment capacity ratio M_y/M_u, the failure mode of flexural strengthened RC beams was divided into two types: flexural compression failure and debonding failure. These findings are well in line with the earlier investigation. As a result, the failure mode of flexural strengthened RC beams with AFRP sheets may be expected based on the computed bending moment capacity ratio M_y/M_u.

4.4 Summary

The failure modes of the RC beams strengthened with AFRP sheets were investigated in this chapter utilizing static loading experiments employing the sheet volume. The conclusions are summarized as follows:

1. When compared to non-strengthened beams, the strengthened beams' capacity to carry loads was greatly increased.

2. Based on the predicted bending moment capacity ratio M_y/M_u, the failure mechanism of flexural strengthened RC beams was divided into two types: flexural compression failure and debonding failure. These findings are fairly consistent with the earlier investigation [21].

3. Flexural failure was the mode of failure for all RC beams, strengthened or not.

4. Sheet debonding caused all of the reinforced RC beams to fail.

Chapter 5: LOW-VELOCITY DROP-WEIGHT IMPACT LOADING TESTS

5.1 Introduction

The development of structures with explosion and impact resistance is necessary due to the substantial threat posed by global terrorist activities and threats to civil infrastructures. In order to enhance RC constructions against static, blast, and impact loads, FRP materials can be employed. A few research [2,3] has been done on the reinforcement of RC structures that have been subjected to blast loads. There have only been a small number of prior studies on the impact resistance of FRP-enhanced RC beams [4, 37, 39–50, 60]. The impact resistance of RC beams using FRP sheets was studied by Kishi et al. [37]. The results of low-velocity impact loading tests on reinforced beams that had AFRP or CFRP sheets bonded to the tension-side surfaces showed that flexural strengthening using FRP sheets can enhance the impact-resistant capacities of such beams. If the axial stiffness values of the sheets are identical, the strengthening effects will be the same regardless of the sheet materials. Erki and Meier [39] examined the dynamic behavior of CFRP laminates or steel plates-reinforced RC beams. Their experiments involved raising one end of a simply supported beam and then dropping it from various heights to produce impact loading. RC beams externally reinforced with CFRP laminates behave well under impact loading, according to the data, however, they are unable to absorb as much energy as beams externally reinforced with steel plates. Non-shear reinforced RC beams that had laminates of either CFRP or Kevlar FRP screwed to their top and bottom surfaces were put through drop-weight impact tests by Tang and Saadatmanesh [40]. The maximum deflection of RC beams was found to be greatly reduced, and their capacity to sustain impact loading was also found to be significantly increased, by the use of composite laminates. Pham and Hao [41] looked into the impact behaviors of RC beams that had been strengthened with FRP and the role that FRP had in shear strength. In their study, they strengthened RC beams without stirrups using CFRP U-wraps and 45°-angle wraps. According to their research, 45°-angle wraps perform better than FRP U-wraps in terms of beam deflections and load-carrying capacities when the same amount of FRP is utilized. Additionally, the ductile flexure failure under static loading was changed to brittle shear failure under impact loading for the RC beams. In order to better understand how CFRP-strengthened RC beams respond to static and impact loads, Pham and Hao [42] employed longitudinal FRP strips and FRP U-wraps. In order to limit the longitudinal FRP strips and lessen the stress concentration on the FRP

U-wraps, curved soffits were added to certain beam sections. The results show that in comparison to rectangular equivalents strengthened with the same volume of FRP, their modification technique greatly increases load-carrying capacities. Additionally, all of the beams statically failed in the pure flexural mode during the impact loading tests, switching to the shear-flexure mode, whereas the strengthened beams failed as a result of the FRP sheet rupturing or debonding. Other investigations [4, 43-50, 60] demonstrated that all RC beams have increased impact-resist capabilities after being strengthened using FRP materials. However, it is yet unknown how the FRP sheet of the reinforced beams fails when subjected to impact pressure.

The effect of FRP volume on the rupture/debonding of FRP sheets in the strengthened beams has not yet been researched, despite the fact that the flexural load-carrying capacity and failure behavior of reinforced RC beams under impact loading have both been examined. Additionally, it hasn't been determined how the input impact energy affects the beam's failure mode. But according to Kishi et al. [21], depending on the predicted bending moment capacity ratio M_y/M_u, the failure mode of flexural strengthened RC beams under static loading was divided into two types: flexural compression failure and debonding failure. In Chapter 4, the outcomes were confirmed. The impact loading scenario has not yet been studied with regard to this failure mode. In addition, the relationship between the failure modes of reinforced RC beams enhanced with FRP sheets under static and impact loading instances has not yet been fully elucidated in the studies mentioned above.

This research concentrates on stirrup-equipped RC beams that statically approach the ultimate state and show flexural failures from this aspect. Low-velocity drop-weight impact loading tests on RC beams reinforced in flexure with AFRP sheets were performed in order to assess the effects of the sheet volume and weight drop height on the failure mode of the beams. The beams' impact resistance, impact-resistant characteristics, and failure behavior were all investigated.

5.2 Experimental method

The samples utilized in this research are listed in Table 5.1. In this table, the nominal names of the specimens are listed with a hyphen after the reinforcing material (N: none, A: AFRP), the kind of loading (I: impact loading), and the weight drop height H*n* (*n*: drop height in metric units). Based on the drop weight (m = 300 kg) and the weight's measured drop velocity (v) just before reaching the top surface of the beam, the actual input energy ($E_i = mv^2/2$) was calculated in Table 5.1.

Table 5.1. List of specimens [51].

Specimen	Set drop height H (m)	Measured drop velocity v (m/s)	Actual input energy E_i (kJ)	Compressive strength of concrete $f_c^{'}$ (MPa)	Yield strength of main rebar f_{ya} (MPa)	Yield strength of stirrup f_{ys} (MPa)	Calculated flexural load capacity P_{usc} (kN)	Calculated shear load capacity V_{usc} (kN)	Shear-flexural capacity ratio α
N-I-H0.5	0.5	3.19	1.53	34.3	394	373	57.1	284	4.97
A415-I- H0.5		3.13	1.46				83.55		3.40
A830-I- H0.5		3.13	1.46				102.2		2.78
A1660-I-H0.5		3.16	1.49				128.2		2.22
N-I-H1.0	1.0	4.58	3.15	34.3	394	373	57.1	284	4.97
A415-I- H1.0		4.45	2.97				83.55		3.40
A830-I- H1.0		4.45	2.97				102.2		2.78
A1660-I-H1.0		4.51	3.06				128.2		2.22
A415-I- H2.0	2.0	6.24	5.85	33.7	371	402	81.0	299	3.69
A830-I- H2.0							99.9		2.99
A1660-I-H2.0							126.1		2.37
N-I-H2.5	2.5	6.70	6.74	32.4	382	462	55.0	329	5.98
A415-I-H2.5		6.99	7.33	33.7	371	402	81.0	299	3.69
A830-I-H2.5							99.9		2.99
A1660-I-H2.5							126.1		2.37
A415-I-H3.0	3.0	7.53	8.50	33.7	371	402	81.0	299	3.69
A830-I-H3.0		7.72	8.95				99.9		2.99
A1660-I-H3.0							126.1		2.37
A415-I-H3.5	3.5	8.15	9.97	34.3	394	373	83.55	284	3.40
A830-I-H3.5		8.39	10.55				102.2		2.78
A1660-I-H3.5							128.2		2.22

The calculated flexural and shear load capacity of the beams was determined similarly to those in Chapter 4. The shear-flexural capacity ratio $\alpha = V_{usc}/P_{usc}$ of all strengthened RC beams is greater than 1.0, which indicates that they should statically reach the flexure failure mode according to Table 5.1.

Figure 3.5 displays the test configuration for the drop-weight impact loading test. By using the results of the previous study [37], the weight's drop heights were determined to be 0.5, 1.0, 2.0, 2.5, 3.0, and 3.5 m.

5.3 Experimental results and discussions for low-velocity drop-weight impact loading

5.3.1 Time histories of impact force, reaction force, and deflection

Figure 5.1 displays the time histories of the impact force *P*, response force *R*, and deflection *D* of the reinforced and unreinforced RC beams made of AFRP sheets in flexure. All of the tested beams' maximum impact force, response force, deflection, and residual deflection are listed in Table 5.2. As indicated in Table 5.1, actual input impact energy is used in this table.

In 25-ms intervals from the time of impact, Figure 5.1a shows the impact force *P*'s time history. Regardless of the sheet volume or weight drop height, it can be seen that the responses of all beams with and without strengthening had comparable time histories. The time history first revealed the first peak at the impact's beginning, which had a triangle form, a high amplitude, and a brief duration (approximately 1 ms). Second, the lesser amplitude, the triangular-shaped second peak was aroused. The maximum impact force increased with the increasing drop height, regardless of the beam (with or without reinforcement with FRP sheets, according to Table 5.2). At the same predetermined drop height, the maximum impact force did, however, increase as flexural stiffness did. Prior to this result, Tang and Saadatmanesh [40] reported it.

The reaction force *R*'s time histories are shown in Figure 5.1b at intervals of 200 ms following impact. Regardless of the sheet volume or weight drop height, it can be seen that the responses of all beams (with or without strengthening) followed similar time courses. Approximately 50 kN of tightening force was stimulated as a negative response force at the start of the impact. This indicates that the cross beams at the support points were tightened in order to stop the beam from rebounding before the amplifier device was balanced to zero. In earlier investigations, this behavior was also mentioned (Kishi et al. [37], Pham and Hao [42], Cotsovos [43]).

With great amplitude and a brief period, the initial triangular-shaped peak was stimulated. After then, smaller amplitudes were used to trigger the subsequent triangular-shaped peaks. Because the strengthened beams had greater bending stiffness, the primary response tended to last longer as drop height increased whereas decreasing sheet volume at the same drop height resulted in shorter time duration. Due to the beam's low-frequency vibration after unloading, the time history after the primary response displayed damped sinusoidal patterns.

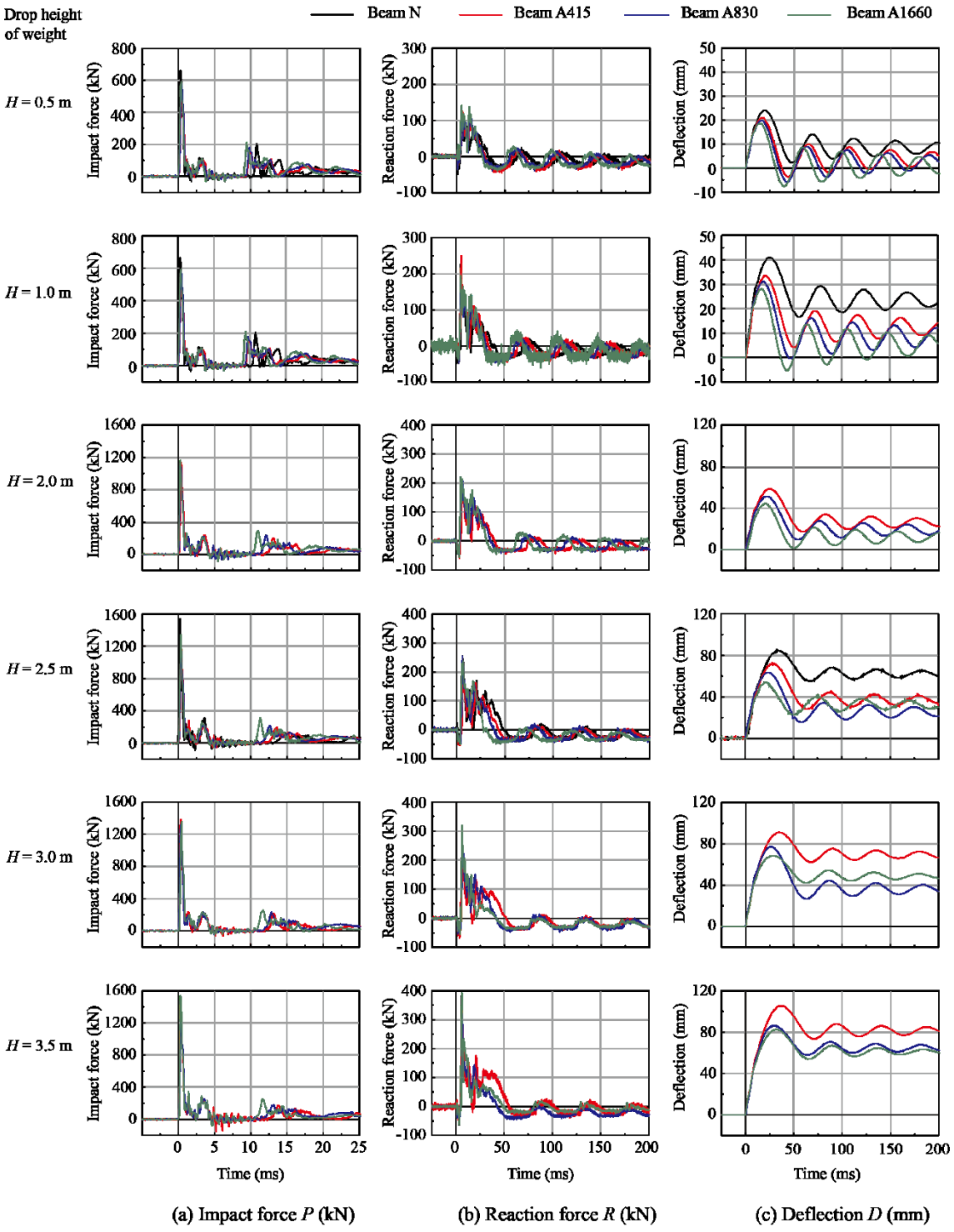

Figure 5.1. Time history of beams' dynamic responses [51].

Table 5.2. Values of RC beams' maximum dynamic response under impact loading [51].

Specimen	Set drop height H (m)	Actual input energy E_i (kJ)	Maximum impact force $P_{\max}$ (kN)	Maximum reaction force $R_{\max}$ (kN)	Maximum deflection $D_{\max}$ (mm)	Residual deflection D_{res} (mm)
N-I-H0.5	0.5	1.53	663	106	24.0	8.5
A415-I- H0.5		1.46	487	130	20.9	3.9
A830-I- H0.5		1.46	587	135	20.0	2.5
A1660-I- H0.5		1.49	595	141	18.8	1.1
N-I-H1.0	1.0	3.15	948	229	40.9	23.0
A415-I- H1.0		2.97	869	250	33.8	12.2
A830-I- H1.0		2.97	771	178	31.6	8.7
A1660-I- H1.0		3.06	863	196	28.0	5.1
A415-I- H2.0	2.0	5.85	1138	209	58.6	26.9
A830-I- H2.0			1103	213	51.7	20.0
A1660-I- H2.0			1165	222	44.5	12.4
N-I-H2.5	2.5	6.74	1542	251	85.9	62.0
A415-I-H2.5		7.33	1165	214	73.1	37.5
A830-I-H2.5			1147	254	65.2	26.4
A1660-I-H2.5			1346	239	54.2	33.3
A415-I-H3.0	3.0	8.50	1387	215	91.1	70.3
A830-I-H3.0		8.95	1324	224	76.6	35.9
A1660-I-H3.0			1356	320	68.5	49.4
A415-I-H3.5	3.5	9.97	1428	331	104.4	80.5
A830-I-H3.5		10.55	1246	323	86.0	64.6
A1660-I-H3.5			1537	393	82.5	61.1

According to Table 5.2, both the non-strengthened and strengthened RC beams had a greater maximum response force as the drop height increased. At the same drop height, as the sheet volume rose, the stresses on the reinforced RC beams increased.

The time histories of deflection D in the first 200 ms following impact are shown in Figure 5.1c. The major reactions are identifiable as half-sine waveforms. Following the first response, the deflection was limited, and the beams demonstrated low-frequency damped free vibration. As drop height H was raised, there was a tendency for the maximum/residual deflection of the beam to increase.

According to the time histories of the beams, the non-strengthened ones showed higher maximum/residual deflections than the strengthened ones for drop heights H = 0.5, 1.0, and 2.5 m.

According to Table 5.2, for the drop height H = 2.5 m, the maximum and residual deflections of the reinforced beams were reduced by around 15 to 35% and 40 to 60%, respectively, in comparison to the non-strengthened beams. By gluing FRP sheets to the tension-side surfaces of the beams, these deflections might be further increased. The maximum deflection for Beam A1660 was the least of the strengthened beams, although the residual deflection was higher than that of Beam A830. This might be because the sheet debonded once the beam had deflected to its maximum.

With increasing sheet volume for drop heights H = 3.0 and 3.5 m, the maximum/residual deflections of the strengthened beams were reduced. However, with the drop height H = 3.0 m, Beam A1660's residual deflection was larger than Beam A830's (Table 5.2). This may be due to the fact that Beam A830's sheet was only partially debonded after the beams reached their maximum deflection, but Beam A1660's sheet was completely debonded.

In light of this, it was made clear that the RC beams strengthened with externally bonded AFRP sheets had better impact resistance in direct proportion to the sheet volume. The sheet debonding is also more obvious the larger the sheet volume. This is consistent with the computed static bending moment ratio value M_y/M_u, showing the aforementioned tendency. Additionally, this implies that as sheet volume increases, M_y/M_u value decreases, resulting in a bigger primary rebar yield area and simpler debonding of sheets.

5.3.2 Crack patterns of RC beams

Following the impact loading testing, Figure 5.2 displays the fracture distributions for all the RC beams, both with and without strengthening.

Flexural fissures appeared in the lower and upper concrete covers and spread along the whole length of the beams. Near the loading zones, diagonal cracks appeared in each case. These events' characteristics were notably different from those of the static loading scenarios (Figure 4.5). The formation of fracture patterns from the upper concrete layer may be caused by flexural waves that are moving in the direction of the fixed beams' support points at the beginning of the impact.

At drop heights, H = 0.5, 1.0, and 2.0 m, the upper concrete cover close to the beams' loading point may be crushed. The damage seemed to rise with the height of the drop. However, as no sheet debonding or fractures were seen, the reinforced beams at these heights did not reach the ultimate state.

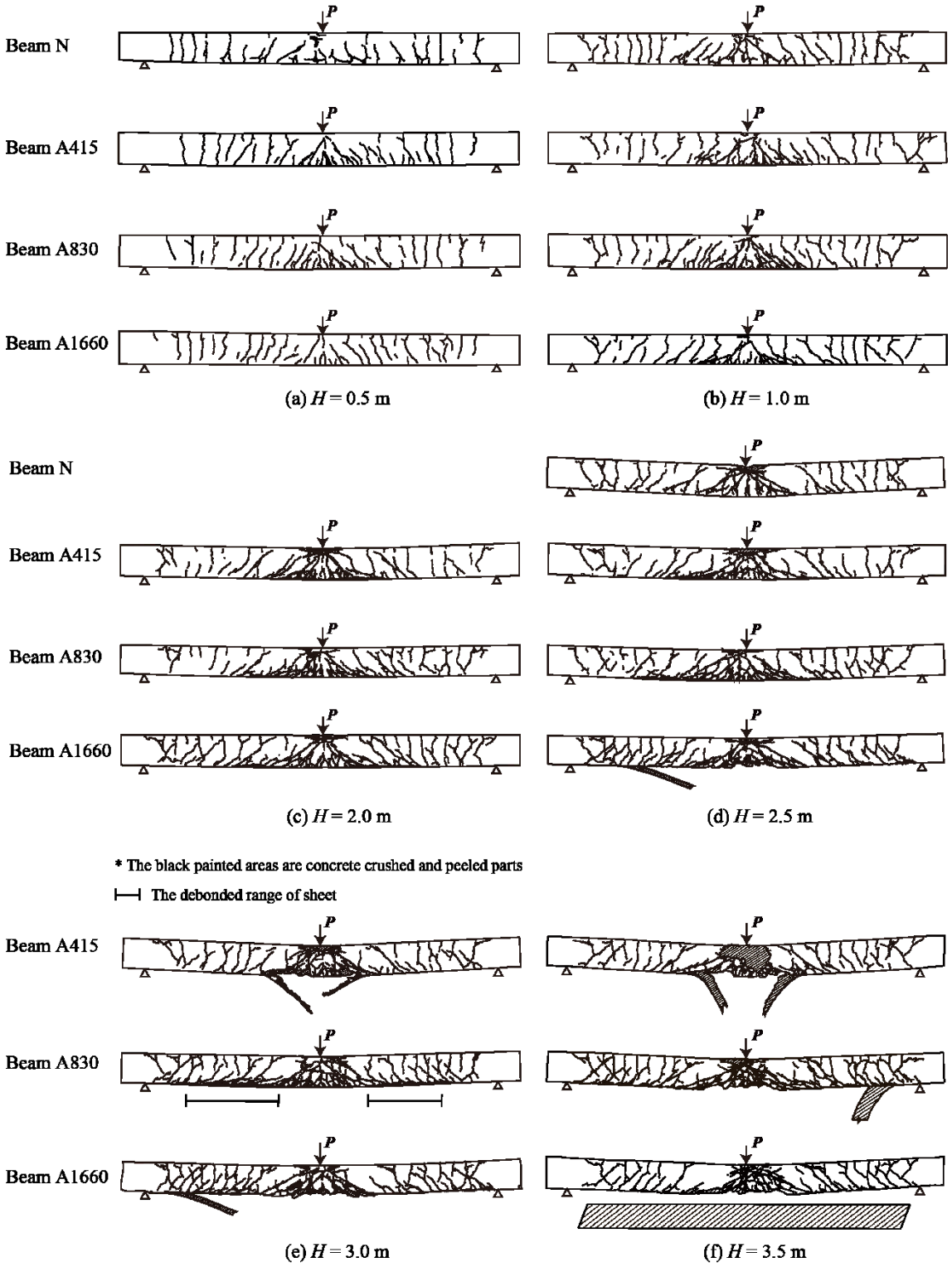

Figure 5.2. Each beam's crack distribution after impact loading tests [51].

At the drop height H = 2.5 m, Beam N reached the final state in the flexural-shear failure mode because the residual displacement was greater than 2% of the beam's pure span. The flexural-shear failure mode was accompanied by a diagonal crack whose tip peeled off, causing the sheet to debond. However, only Beam A1660, which contained the largest volume of sheet among the strengthened beams, reached the ultimate state. The second section explores this phenomenon in depth.

In this experiment, reinforced beams were tested at drop heights of 0.5, 1.0, 2.0, 2.5, 3.0, and 3.5 m. Due to the restricted number of specimens available, studies for Beam N were carried out at drop heights of 0.5, 1.0, and 2.5 m. However, at a drop height of 2.5 m, Beam N's residual displacement was 62 mm (Table 5.2), which was larger than 2% of the clear span (60 mm). As a result, no additional experiments at higher drop heights in Beam N were conducted after Beam N attained its maximum state, according to this result.

In accordance with the findings, all strengthened RC beams obtained their optimum state at drop heights H = 3.0 and 3.5 m. Although both types of beam failure were observed, the damage did get worse with higher drop heights. Beam A415 failed due to sheet rupture, whereas Beam A830/1660 failed due to sheet debonding.

According to the findings, 1) under impact loading, RC beams with or without FRP sheets reached their final state in the flexural-shear failure mode, and 2) the failure mode of strengthened beams relies on the sheet volume and can be separated into two categories, sheet rupturing and sheet debonding. Also, 3) the flexural-reinforced RC beams didn't break when the impact energy was less than 5.85 kJ, which is the same as a drop height of 2.0 m. For Beam A1660 and Beam A415/830, they may not function when the drop height is $H \geq 2.5$ m and $H \geq 3.0$ m, respectively.

5.3.3 Strain distribution of AFRP sheet and crack pattern near loading point

The axial strain distribution of the AFRP sheet and the distribution of cracks on the side close to the loading point of Beams A415/830/1660 at the predetermined drop height H = 3.0 m are depicted in Figure 5.3.

The figure shows that at time t = 0.5 ms following the commencement of impact, many diagonal cracks appeared from both sides of the beams, however, Beams A830/1660 had no flexural cracks yet. There were no cracks identified in Beam A415 however. While compressive strain was produced on both of the loading point's outer borders, the tensile strain was dispersed throughout the midspan of the beams. The development of the fixed ends may be to blame for the development of the compressive

strain. It was determined that the tension eventually moved toward both support points. The strain of the sheet beneath the loading point for Beam A415 and Beam A830/1660 was 0.5% and 0.25%, respectively.

At time t = 1.0 ms, all diagonal cracks had extended to the lower concrete cover's margins, and Beams A830/1660 had developed flexural cracks. Although Beam A415 had a number of diagonal fissures, they had not yet extended to the borders of the lower concrete cover. For all beams, positive and negative strains migrated toward the opposing support points. Furthermore, Beams A830/1660's equi-bending tendency caused the tensile strain to be spread uniformly close to the loading area. The deformation curvatures in this region may be similar, according to this.

Beam A415 developed a number of new diagonal cracks between times t = 1.5 and 5.0 ms, and each of the diagonal cracks extended to the lower concrete cover's margins. All beams transitioned from the fixed state to the simply supported state in accordance with the strain distributions as the compressive strain spread to the support points on both sides. Furthermore, whereas the strains in Beam A415 were triangularly distributed close to the loading point, they were practically parabolically spread across the whole span in Beams A830/A1660. Beams A415 and A830/1660's different strain distribution forms could be connected to the sheet's failure modes. At time t = 7.5 to 10 ms, all of the beams' midspan regions experienced the development of fresh diagonal and flexural cracks. Additionally, failures due to compression were noted at the top concrete coverings, close to the loading locations for Beams A830/1660. At the midspan, Beam A415 had a distributed strain of about 1.5%, and the strain gradients around the loading point and support point were very different from one another. In contrast, diagonal cracks were dispersed across a large area and tensile strains of around 1% were equally distributed near the loading point for Beams A830/1660. According to high-speed camera images, this is proof that the sheet debonded as a result of the diagonal fractures' tips peeling in the direction of the support points.

For Beam A415 at time t = 15 ms, the FRP sheet experienced a strain of over 2% just below the loading point, and it is clear from the high-speed camera image that the sheet ruptured. Regarding Beam A830, the strain was dispersed in an area of approximately 0.75 m on both sides at the loading point, with a concentration of greater than 0.5%. Due to a different gradient of the strain distribution here than it was close to the support point, the primary rebar was in a plastic state throughout a large range. It can also be proved that 1) the highest strain was close to the sheet's ultimate strain, reaching

about 1.5% right below the loading point. Additionally, 2) under the peeling action of the diagonal cracks' tips, the FRP sheet of the beam tended to debond in the direction of the support points. An area of 1 m on either side of the loading point for Beam A1660 showed a uniform strain distribution with more than 0.5%, indicating that the primary rebars gave way over a larger area than in the case of Beam A830. The highest strain at the loading point was significantly less than that at time t = 10 ms, coming in at about 1%. It is evident from the high-speed camera image that the FRP sheet also exhibited a tendency to debond as a result of the diagonal fractures' tips peeling in the direction of the support points. For Beam A1660, the sheet at the right side of the beam debonded at time t = 20 ms as a result of the diagonal cracks' tips peeling. With regard to Beam A830, a homogeneous strain distribution was found over the whole span at time t = 30 ms, with the exception of areas that were 0.5 m from both supporting points, where it was evident that the sheet was more likely to partially peel off.

Based on these findings, Beam A415's sheet ruptured in less than 15 ms because the upper concrete cover at the loading location was severely crushed and the beam had a V-shaped midspan deformation. As a result of the large sheet volume and low static bending moment capacity ratio M_y/M_u, the primary rebar for Beams A830/1660, on the other hand, tended to be in a plastic condition over a vast region. A tendency for debonding the sheet was also present because of the shallow angle of the diagonal cracks and the considerable peeling activity of the diagonal crack tips.

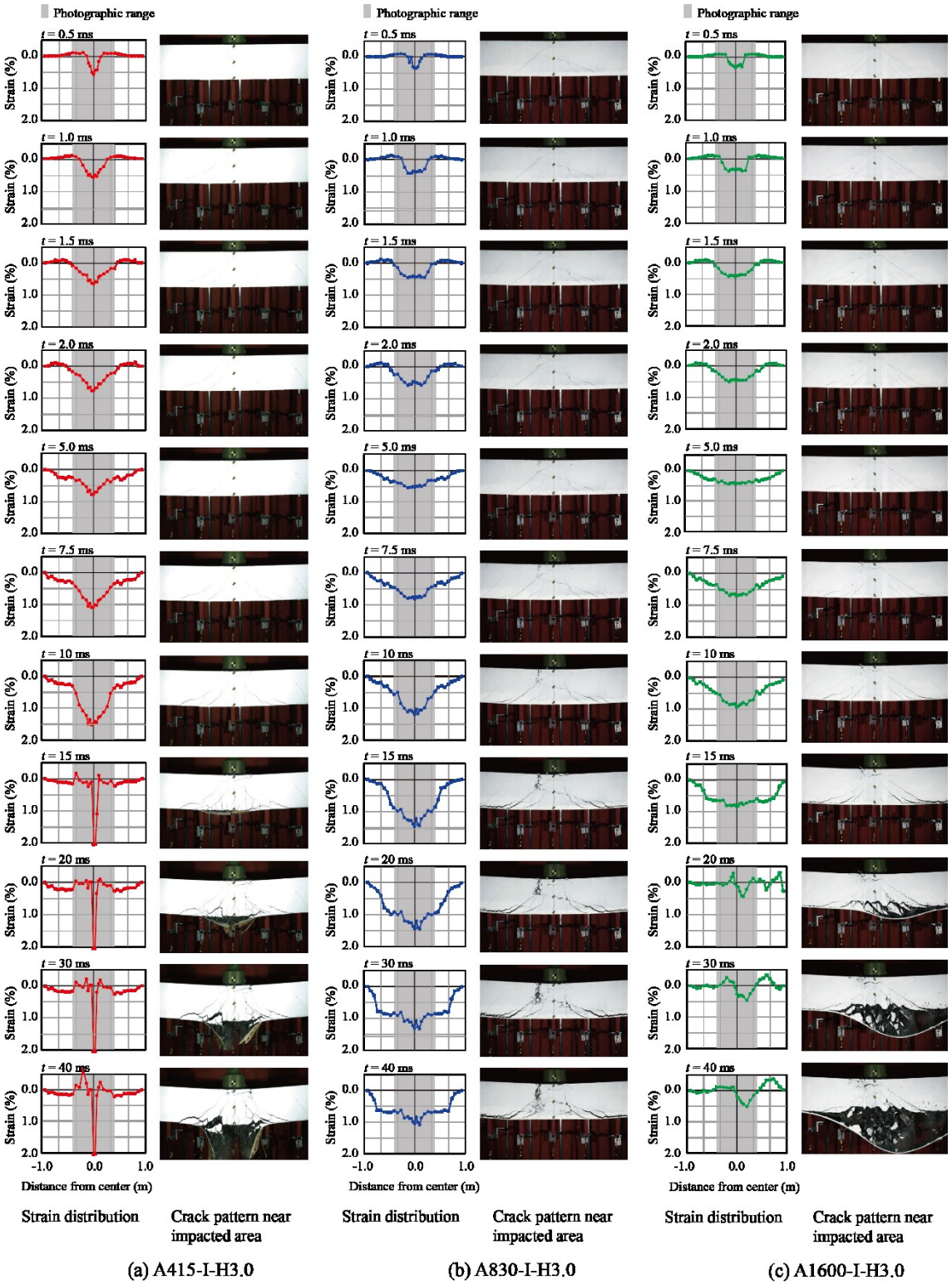

Figure 5.3. Temporal transform of AFRP material's strain distribution and crack forms close to the loading point for height drop H = 3.0 m [51].

5.3.4 Relationship between maximum response values and input impact energy

The maximum/residual deflection and actual input impact energy of the RC beams when subjected to impact loading are depicted in Figures 5.4(a) and (b) in relationships. With the exception of the reinforced beams, which failed due to the sheet debonding or rupturing, it can be seen that the maximum/residual deflection tended to grow linearly with the input impact energy for each beam. In comparison to non-reinforced beams, the slope of strengthened beams was lower, and the slope reduced as the sheet volume increased. As a result, when compared to non-strengthened beams with the same input impact energy, the maximum and residual deflections of the strengthened beams may be limited to roughly 15 to 35% and 40 to 85%, respectively (Table 5.2).

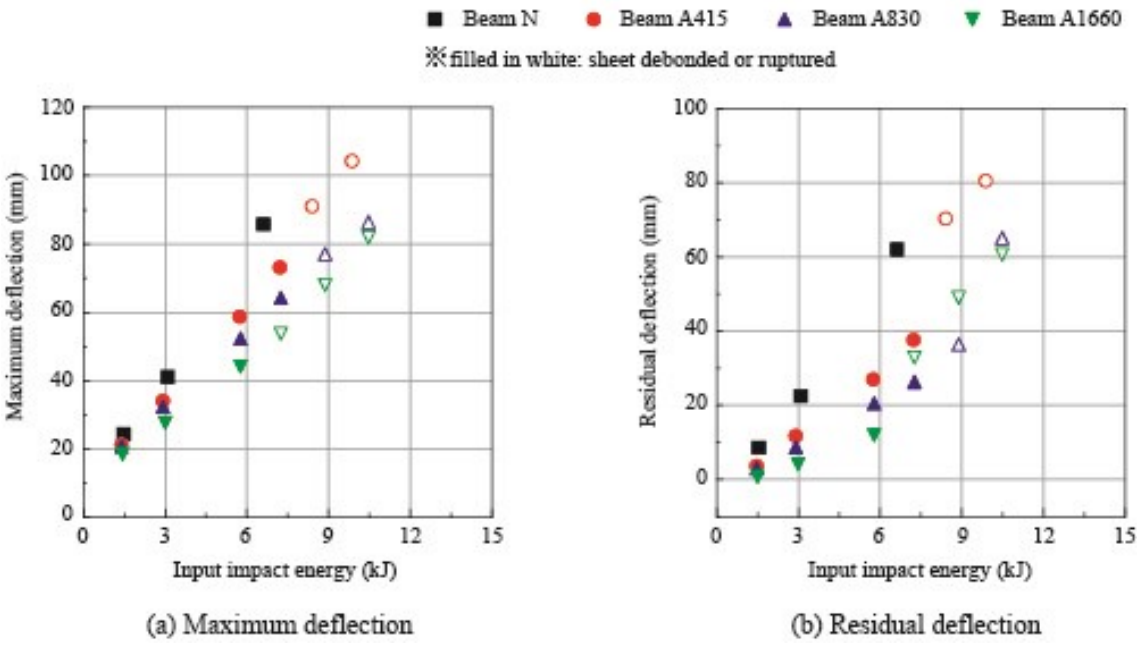

Figure 5.4. Maximum/residual deflection and input impact energy relationships [51].

5.3.5 Failure modes of RC beams strengthened in flexure

The failure modes of the flexurally strengthened RC beams during static and impact loading testing are listed in Table 5.3. It also displays the computed bending moment capacity ratio M_y/M_u, which was employed as an index to forecast the modes of failure under static loading.

Table 5.3 A list of each beam's flexure-enhanced failure mechanisms under various loading conditions [51].

Specimen	Mass per unit area of sheet (g/m^2)	Static calculated bending moment capacity ratio M_y/M_u	Failure mode in the case of static loading	Failure mode in the case of impact loading					
				H = 0.5 (m)	H = 1.0 (m)	H = 2.0 (m)	H = 2.5 (m)	H = 3.0 (m)	H = 3.5 (m)
A415	415	0.71	Flexural compression failure	-	-	-	-	Rupture	Rupture
A830	830	0.62	Debonding failure	-	-	-	-	Partial debonding	Debonding
A1660	1660	0.55	Debonding failure	-	-	-	Debonding	Debonding	Debonding

As was previously mentioned, the calculated bending moment capacity ratio M_y/M_u, as reported in the prior study [21], can be used to predict the failure mode in the static loading case. This prediction agrees well with the experimental data of all the flexurally reinforced RC beams considered here.

Additionally, it was established that "sheet rupturing" was the failure mode under impact loading when the failure mechanism of the reinforced beam with FRP sheets under static stress was expected to be "flexural compression failure." Although "debonding failure" was predicted as the beam's failure mode under static loading, "sheet debonding" was actually the mode of failure under impact loading. Due to the tiny yield area of the primary rebar and the compressive failure of the upper concrete cover, the "sheet rupturing" failure may have been brought on by the V-shaped deformation of the beam. Only Beam A1660, when compared to the other two beams strengthened with various sheet volumes, achieved the ultimate condition with the sheet debonding at the drop height H = 2.5 m. Increasing the sheet volume may therefore not always result in an increase in impact resistance.

A comparison of the crack patterns of the beams under static and impact loads reveals the following: 1) In the static load case, the crack patterns of the beams consist solely of flexural cracks originating from the lower concrete covers, and all beams failed with the flexural failure mode, regardless of whether they were strengthened or not. 2) In the case of an impact load, the beams' crack patterns included flexural cracks emerging from the lower and upper concrete coatings as well as diagonal cracks forming close to

the loading area; both reinforced and unreinforced beams collapsed under a flexural-shear failure mode. Consequently, 3) the failure mode of the RC beams changed from flexural failure under static loads to flexural-shear failure under impact loads, independent of whether the RC beams were strengthened with AFRP sheets.

5.4 Summary

This chapter concentrated on using FRP materials to improve current RC constructions' impact resistance. In order to investigate the enhancement of impact-resistant beams and/or to forecast the failure modes of the RC beams strengthened with AFRP sheets, drop-weight impact loading experiments were carried out. Each beam underwent a single loading procedure for the impact loading tests, and the weight drop height was increased until the sheets broke or debonded. In order to assess the impact of utilizing FRP materials on the flexural strengthening of the RC beams, three different types of AFRP sheets with varying volumes were tested and externally attached to the bottom surfaces of the beams. The results are summarized as follows:

1. In comparison to non-reinforced beams, the maximum and residual displacement of the strengthened beams can be limited by up to 35% and 85%, respectively.

2. The maximum/residual displacement of the RC beams with/without AFRP sheets rose linearly when impact energy was added.

3. Based on the volume of the sheets, the failure mode of the reinforced RC beams was divided into two types: sheet rupturing and sheet debonding. The former is equivalent to the failure mode for flexural compression, whereas the latter is equivalent to the failure mode for debonding under static loading.

4. Whether or not the RC beams were strengthened with AFRP sheets, the failure mechanism of RC beams shifted from flexural failure under static loading to flexural-shear failure when subjected to impact loading.

5. Regardless of static or impact loads, increasing the sheet volume might not help the debonding of the AFRP sheet of the reinforced RC beams.

6. When the input impact energy was more than or equal to 7.33 kJ (corresponding to the drop height H = 2.5 m), the strengthened beams under test failed due to sheet debonding and/or rupturing.

Chapter 6: CONSECUTIVE DROP-WEIGHT IMPACT LOADING TESTS

6.1 Introduction

The AFRP sheets were used in Chapter 5 to strengthen RC beams when they were subjected to impact loads. For each beam, a single loading technique was used during the studies. Investigation and discussion were conducted about the impact of the sheet volume and the input impact energy.

However, in actual use, RC structures may be exposed to a series of impact loads that increase in energy. Consecutive drop-weight impact loading tests on the RC beams strengthened in flexure with externally bonded AFRP sheets were carried out as part of the study's investigation of the impact-resistant properties of the RC members in this chapter. To assess the strengthening effect of beams, the sheet volume and cumulative input impact energy were examined. 415, 830, and 1660 g/m^2 sheets were utilized. In order to reach the beam's equivalent ultimate state, the drop height of the weight was increased by 1.0, 2.0, 2.5, and 3.0 m. Additionally assessed as a reference were unreinforced beams. On the basis of the test results, relationships between maximum/residual deflections and the input impact energy were explored, as well as the failure behavior of the beams.

6.2 Experimental method

The study's sample list can be found in Table 6.1. The computed flexural and shear load-carrying capacities of the specimens, as well as the weight's drop height, impact energy input, and concrete and rebar material parameters, are displayed. The nominal name of the specimen was given in the following table together with the strengthening material (N: none and AS: AFRP), loading method (CI: consecutive impact loading), and set drop height of the weight (*Hm-n*) (*m* and *n*: drop height for the initial and subsequent loadings, respectively, in metric unit). The predicted flexural and shear load capacities of the beams as well as the actual input energy were determined similarly to those provided in Table 5.1 and are shown in Table 6.1.

The failure of Beam A415 involved a sheet rupture, as shown in Table 6.1. whereas the sheet debonding caused by Beams A830/A1660 caused the failure.

Figure 3.5 displays the test configuration for the drop-weight impact loading test. Until the beams achieved their final state as a result of the AFRP sheet debonding or fracturing, the drop height was raised by a factor of 1.0, 2.0, 2.5, and 3.0 m.

Table 6.1. List of specimens.

Specimen	Experimental case	Set drop height of weight H (m)	Measured drop velocity v (m/s)	Actual input impact energy E_i (kJ)	Accumulated input impact energy E_{ai} (kJ)	Compressive strength of concrete $f_c^{'}$ (MPa)	Yield stress of axial rebar f_{ya} (MPa)	Yield stress of stirrup f_{ys} (MPa)	Calculated flexural load capacity P_{usc} (kN)	Calculated shear load capacity V_{usc} (kN)	Failure of AFRP sheet
N-CI-H1	N-CI-H1-1	1	4.45	2.97	2.97	33.7	371.0	401.9	54.0	298.8	-
	N-CI-H1-2	2	6.24	5.85	8.82						-
N-CI-H2.5	N-CI-H2.5-2.5	2.5	6.99	6.73	6.73	32.4	381.7	461.9	55.0	329.0	-
A415-CI-H1	A415-CI-H1-1	1	4.45	2.97	2.97	33.7	371.0	401.9	81.0	298.8	-
	A415-CI-H1-2	2	6.12	5.61	8.58						Rupture
A415-CI-H2	A415-CI-H2-2	2.0	6.24	5.85	5.85						-
	A415-CI-H2-2.5	2.5	6.99	7.33	13.18						Rupture
A415-CI-H2.5	A415-CI-H2.5-2.5	2.5	6.99	7.33	7.33						-
	A415-CI-H2.5-3.0	3.0	7.72	8.95	16.28						Rupture
A415-CI-H3	A415-CI-H3.0	3.0	7.53	8.50	8.50						Rupture
A830-CI-H1	A830-CI-H1-1	1	4.45	2.97	2.97	33.7	371.0	401.9	99.9	298.8	-
	A830-CI-H1-2	2	6.12	5.61	8.58						-
	A830-CI-H1-2.5	2.5	6.99	7.33	15.91						Debonding
A830-CI-H2	A830-CI-H2-2	2.0	6.24	5.85	5.85						-
	A830-CI-H2-2.5	2.5	6.99	7.33	13.18						Debonding
A830-CI-H2.5	A830-CI-H2.5-2.5	2.5	6.99	7.33	7.33						-
	A830-CI-H2.5-3.0	3.0	7.72	8.95	16.28						Debonding
A830-CI-H3	A830-CI-H3.0	3.0	7.72	8.95	8.95						Debonding
A1660-CI-H1	A1660-CI-H1-1	1	4.45	2.97	2.97	33.7	371.0	401.9	126.1	298.8	-
	A1660-CI-H1-2	2	6.24	5.85	8.82						-
	A1660-CI-H1-2.5	2.5	6.99	7.33	16.15						Debonding
A1660-CI-H2	A1660-CI-H2-2	2.0	6.24	5.85	5.85						-
	A1660-CI-H2-2.5	2.5	7.15	7.69	13.54						Debonding
A1660-CI-H2.5	A1660-CI-H2.5	2.5	6.99	7.33	7.33						Debonding
A1660-CI-H3	A1660-CI-H3.0	3.0	7.72	8.95	8.95						Debonding

6.3 Experimental results for consecutive drop-weight impact loading

6.3.1 Time histories of impact force, reaction force, and deflection

6.3.1.1 Beams N-CI-H1 and AS-CI-H1

The time histories of the impact force *P*, the response force *R*, and the deflection *D* between Beams N-CI-H1 and AS-CI-H1 are compared in Figure 6.1.

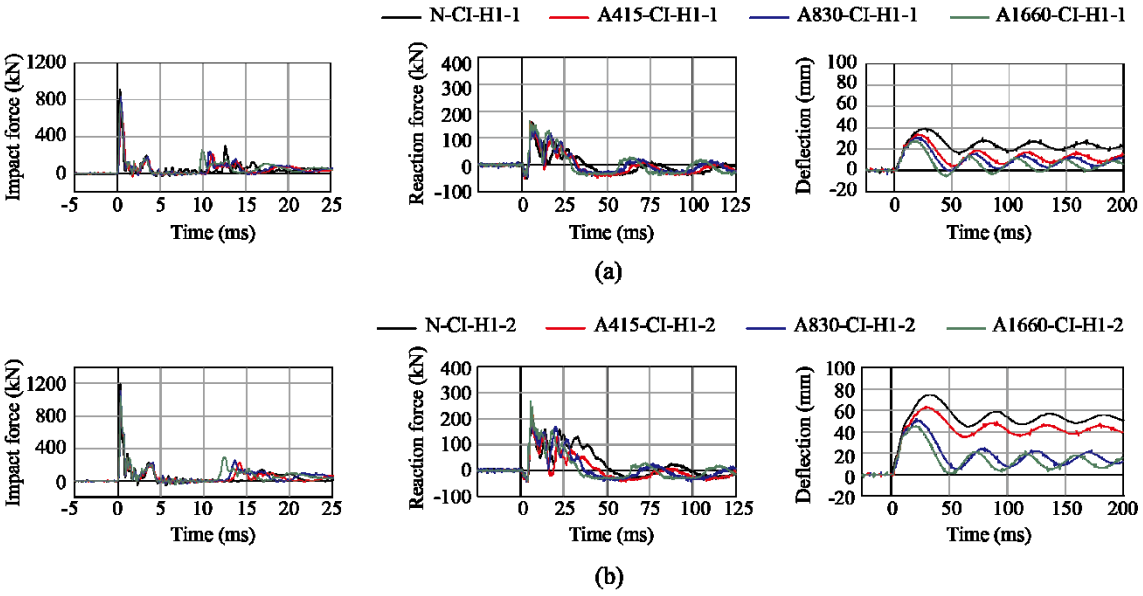

Figure 6.1. Comparisons of time histories of impact force *P*, reaction force *R*, and deflection *D* between Beams N and AS:
(a) Beam N/AS-CI-H1-1; and (b) Beam N/AS-CI-H1-2.

Figure 6.1a compares the dynamic responses between Beams N/AS-CI-H1 at the drop height H = 1 m. It can be seen from the figures that: 1) the time histories of the primary response to the impact force *P* and the reaction force *R* were comparable; however, 2) the maximum and residual deflections for Beam AS were smaller than those of Beam N. In Table 6.2, maximum dynamic response values are listed.

Figure 6.1b compares the dynamic responses between Beams N/AS-CI-H1 at the drop height H = 2.0 m. The following can be seen from these figures: 1) The time histories of the impact force P were comparable; 2) the major response of the reaction force *R* for Beam N had a longer time length compared to Beam AS; and 3) the maximum and residual deflections for Beam AS were likewise noticeably less than those for Beam N.

This figure shows that Beam AS's maximum and residual deflections were significantly better than those of Beam N. The sheet volume and the strengthening impact were correlated.

6.3.1.2 Beam AS at different impact loading steps

Table 6.2. Values of RC beams' maximum dynamic response under consecutive impact loading.

Specimen	Experimental case	Set drop height of weight H (m)	Accumulated input impact energy E_{ai} (kJ)	Maximum impact force $P_{\max}$ (kN)	Maximum reaction force $R_{\max}$ (kN)	Maximum deflection $D_{\max}$ (mm)	Residual deflection D_{res} (mm)
N-CI-H1	N-CI-H1-1	1	2.97	912	159	39.8	23.6
	N-CI-H1-2	2	8.82	1202	210	74.4	52.9
N-CI-H2.5	N-CI-H2.5-2.5	2.5	6.73	1542	250	85.8	62.7
A415-CI-H1	A415-CI-H1-1	1	2.97	766	160	34	12.6
	A415-CI-H1-2	2	8.58	1044	215	64	42.4
A415-CI-H2	A415-CI-H2-2	2.0	5.85	1138	209	58.6	26.9
	A415-CI-H2-2.5	2.5	13.18	629	277	79	54.7
A415-CI-H2.5	A415-CI-H2.5-2.5	2.5	7.33	1165	214	73.1	37.5
	A415-CI-H2.5-3.0	3.0	16.28	663	302	87.5	63.9
A415-CI-H3	A415-CI-H3.0	3.0	8.50	1386	215	89.5	68.5
A830-CI-H1	A830-CI-H1-1	1	2.97	833	150	30.6	8.8
	A830-CI-H1-2	2	8.58	1115	229	52.5	15.9
	A830-CI-H1-2.5	2.5	15.91	794	278	69.9	46.8
A830-CI-H2	A830-CI-H2-2	2.0	5.85	1103	213	51.7	20
	A830-CI-H2-2.5	2.5	13.18	988	286	72.3	49.1
A830-CI-H2.5	A830-CI-H2.5-2.5	2.5	7.33	1147	254	65.2	26.4
	A830-CI-H2.5-3.0	3.0	16.28	657	291	94.9	69.5
A830-CI-H3	A830-CI-H3.0	3.0	8.95	1324	224	76.6	35.9
A1660-CI-H1	A1660-CI-H1-1	1	2.97	766	164	27.7	5.4
	A1660-CI-H1-2	2	8.82	1047	264	45.2	12.3
	A1660-CI-H1-2.5	2.5	16.15	786	280	81.3	57.7
A1660-CI-H2	A1660-CI-H2-2	2.0	5.85	1165	222	44.5	12.4
	A1660-CI-H2-2.5	2.5	13.54	1204	285	77.6	53.6
A1660-CI-H2.5	A1660-CI-H2.5	2.5	7.33	1346	239	54.2	33.3
A1660-CI-H3	A1660-CI-H3.0	3.0	8.95	1356	320	68.5	49.4

In Figures 6.2, 6.3, and 6.4, time histories on dynamic responses for each Beam AS are compared between two successive loading phases. The accumulated answers from subsequent loadings have not been included in these comparisons because each time history was only for the specific loading phase. The responses, regardless of the size of the initial and successive drop heights, are seen to have comparable time histories in the figures, with the exception of the maximum amplitude, the primary response's duration, and the damped-free vibration period for the beam after unloading. In Table 6.2, the highest response values for all beams are displayed.

These graphs show that the negative response forces were present at the impact's early stages. Accordingly, the rebound could cause the beams' two ends to be elevated.

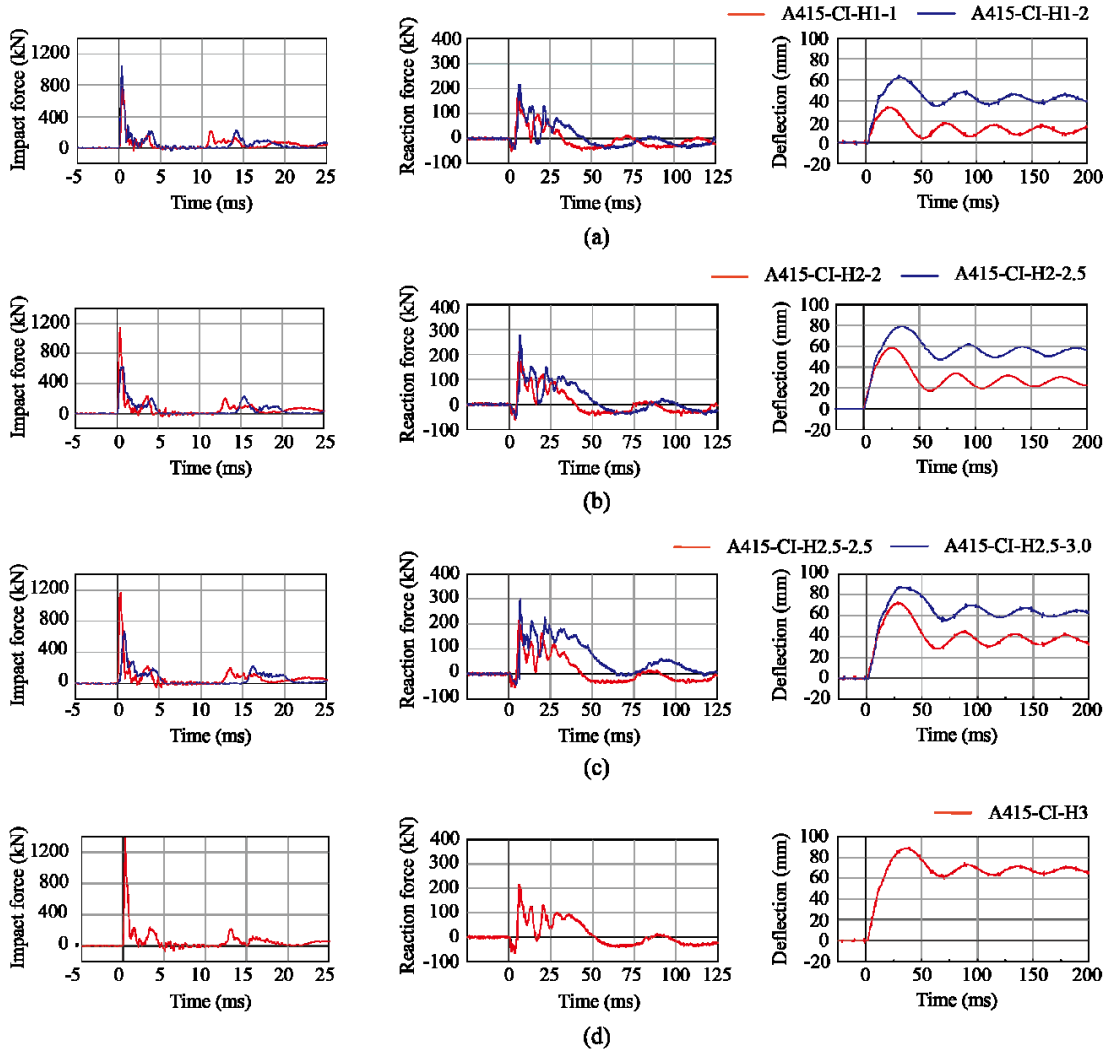

Figure 6.2. Comparisons of Beam A415's impact force *P*, reaction force *R*, and deflection *D* time histories: (a) Beam A415-CI-H1; (b) Beam A415-CI-H2; (c) Beam A415-CI-H2.5; and (d) Beam A415-CI-H3.

Figure 6.2 compares the time histories of the dynamic responses for every Beam A415 throughout successive loading steps.

Experimental comparisons for Beam A415-CI-H1 are shown in Figure 6.2a. The results are shown in this figure, which show that: 1) the minimum and maximum impact forces excited at the drop heights H = 1.0 m and H = 2.0 m were 766 kN and 1044 kN, respectively; 2) the maximum reaction force tends to increase with increasing the drop height H; and 3) the time duration of the main response of the reaction force R for the case at H= 2.0 m was prolonged for 15 ms compared with that at H = 1.0 m because of the sheet debonding.

According to the results of the deflection time histories, maximum and residual deflections for each loading step grew as the succeeding drop height H rose, and the natural period of the damped-free vibration also lengthened in a manner comparable to this. However, given the residual deflection at H = 2.0 m was roughly four times more than it was at H = 1.0 m, this indicates that the sheet ruptured at this loading stage.

Comparisons of the experimental findings for Beam A415-CI-H2 are shown in Figure 6.2b. Due to the AFRP sheet rupturing in this instance, the beam reached its final state at the drop height H = 2.5 m. The following finding may be deduced from these figures: With increasing drop height H, the maximum impact force reduced but the reaction force increased. Additionally, the major response at H = 2.5 m took 15 ms longer to complete than at H = 2.0 m due to the AFRP sheet rupturing. When beams A415-CI-H1 (see Figure 6.2a) and beam A415-CI-H2 were compared for maximum and residual deflections at drop heights of H = 2.0 m, it was discovered that: 1) the maximum deflections were nearly identical; however, 2) the residual deflections for beam A415-CI-H1 were noticeably larger than that for beam A415-CI-H2. Because of the AFRP sheet rupturing at H = 2.0 m, Beam A415-CI-H1 failed.

The experimental results for Beam A415-CI-H2.5 are displayed in Figure 6.2c. In this instance, the second loading phase (H = 3.0 m) marked the end of the impact test. The sheet ruptured, which caused the beam to fail. Beam A415-CI-responses H2.5's tended to be comparable to those of Beam A415-CI-H2.0. When comparing the maximum and residual deflections of Beams A415-CI-H2 (see Figure 6.2b) and Beam A415-CI-H2.5 at the drop heights H = 2.5 m, it can be noted that they had bigger maximum/residual deflections than Beam A415-CI-H25. This is because Beam A415-CI-H2 suffered greater damage as a result of repeated loading.

The experimental findings for Beam A415-CI-H3 are displayed in Figure 6.2d. Because the AFRP sheet broke at this loading stage, the impact test in this instance was terminated after the initial load was applied. When comparing the dynamic reactions to Beam A415-CI-H2.5 at H = 3.0 m, it can be noticed that: 1) the maximum impact force was about doubled. This is because 1) Beam A415-CI-H2.5 suffered severe damage at this drop height, 2) the response force was lower than for Beam AS-CI-H2.5, and 3) the maximum and residual deflections were comparable.

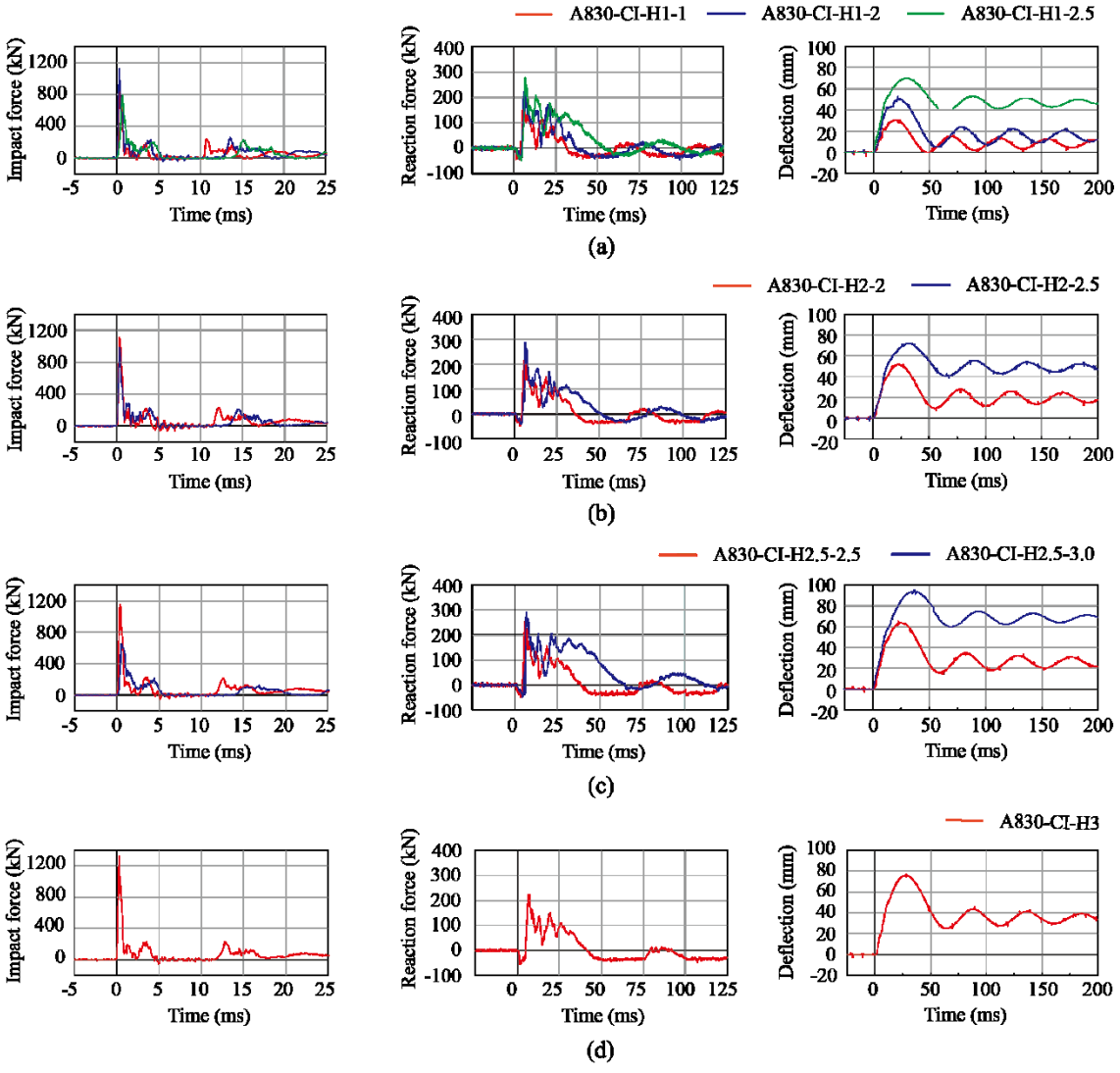

Figure 6.3. Comparisons of Beam A830's impact force P, reaction force R, and deflection D time histories: (a) Beam A830-CI-H1; (b) Beam A830-CI-H2; (c) Beam A830-CI-H2.5; and (d) Beam A830-CI-H3.

The impact force, reaction force, and deflection time histories for each strengthened Beam A830 during successive loading steps are contrasted in Figure 6.3. The findings show that 1) the time histories for each impact force, reaction force, and deflection are quite similar, with the exception of the maximum amplitude and time duration of the primary response, and 2) the damped-free vibration period for the beam after unloading has a natural vibration period.

The experimental findings for Beam A830-CI-H1 are displayed in Figure 6.3a. From this figure, it can be seen that the greatest and least impact forces were 1,120 kN and 790 kN, respectively, and were stimulated at the weight's drop height H = 2.0 m and 2.5 m, respectively. According to the reaction force time histories R, the maximum response force tends to rise as the drop height H rises. When compared to the scenario where H = 2.0 m, the major response's time length for the case where H = 2.5 m was 15 ms longer. The debonding of the sheet may be to blame for this phenomenon. The time history for the deflection for the drop height H = 2.5 m has partially vanished because the laser beam used to measure the deflection may be disrupted by the little concrete blocks of the lower concrete cover debonding and collapsing. The following information can be seen from these time histories: 1) Even though the AFRP sheet debonded at the drop height H = 2.5 m, maximum and residual deflections for each loading step increased with increasing drop height H, and the natural time of the damped-free vibration was similarly prolonged; 2) the time history did not clearly demonstrate that influence; and 3) however, it is indicated that the sheet debonded at this loading stage since the residual deflection at H = 2.5 m was three times more than it was at H = 2.0 m.

Figure 6.3b displays the experimental findings for Beam A830-CI-H2. The beam attained its final state at the drop height H = 2.5 m in this example due to the AFRP sheet debonding. These numbers show that the maximum reaction force increased with drop height H, despite the fact that the maximum impact force at H = 2 m was greater than that at H = 2.5 m. Relative deflections between Beams A830-CI-H1 (Fig. 6.3a) and A830-CI-H2 at the same drop heights H = 2.0 and 2.5 m were similar, although the maximum deflection at H = 2.0 m for the A830-CI-H2 was around 15 mm smaller than that for the A830-CI-H1. Therefore, even if the RC beams were reinforced with the AFRP sheet, damage from subsequent loading may still occur.

Figure 6.3c displays the experimental outcomes for Beam A830-CI-H2.5. In this instance, the AFRP sheet did not debond at H = 2.5 m, but rather debonded and arrived at the final state at H = 3.0 m. According to these calculations, the beam may sustain

substantial damage at H = 3 m because the maximum impact force is nearly half that at H = 2.5 m.

At H = 3.0 m, the maximum reaction force was larger than at H = 2.5 m, and the major response lasted for 25 ms longer at H = 3.0 m than it did at H = 2.5 m. This can be the result of the AFRP sheet debonding. According to the results of deflection time histories, the maximum and residual deflections of the beam at H = 2.5 m substantially decreased when compared to those of the beams at H = 2.5 m under subsequent loading with H = 1.0 and 2.0 m of the initial load (Beams A830-CI-H1-2.5 and A830-CI-H2-2.5). Because in the latter circumstances, the AFRP sheets debonded, but they did not in the earlier.

Figure 6.3d displays the Beam A830-CI-H3 experimental findings. The impact test was finished after the initial load was applied since the AFRP sheet debonded during this loading phase. These numbers indicate that the maximum impact force was close to 1300 kN. On the other hand, the maximum reaction force was roughly 220 kN, which is comparable to the drop height H = 2.5 m of Beam A830-CI-H2.5. These are assumed to be the outcome of the debonding of the AFRP sheet. At H = 2.5 m, the maximum and residual deflections were marginally higher than those of Beam A830-CI-H2.5.

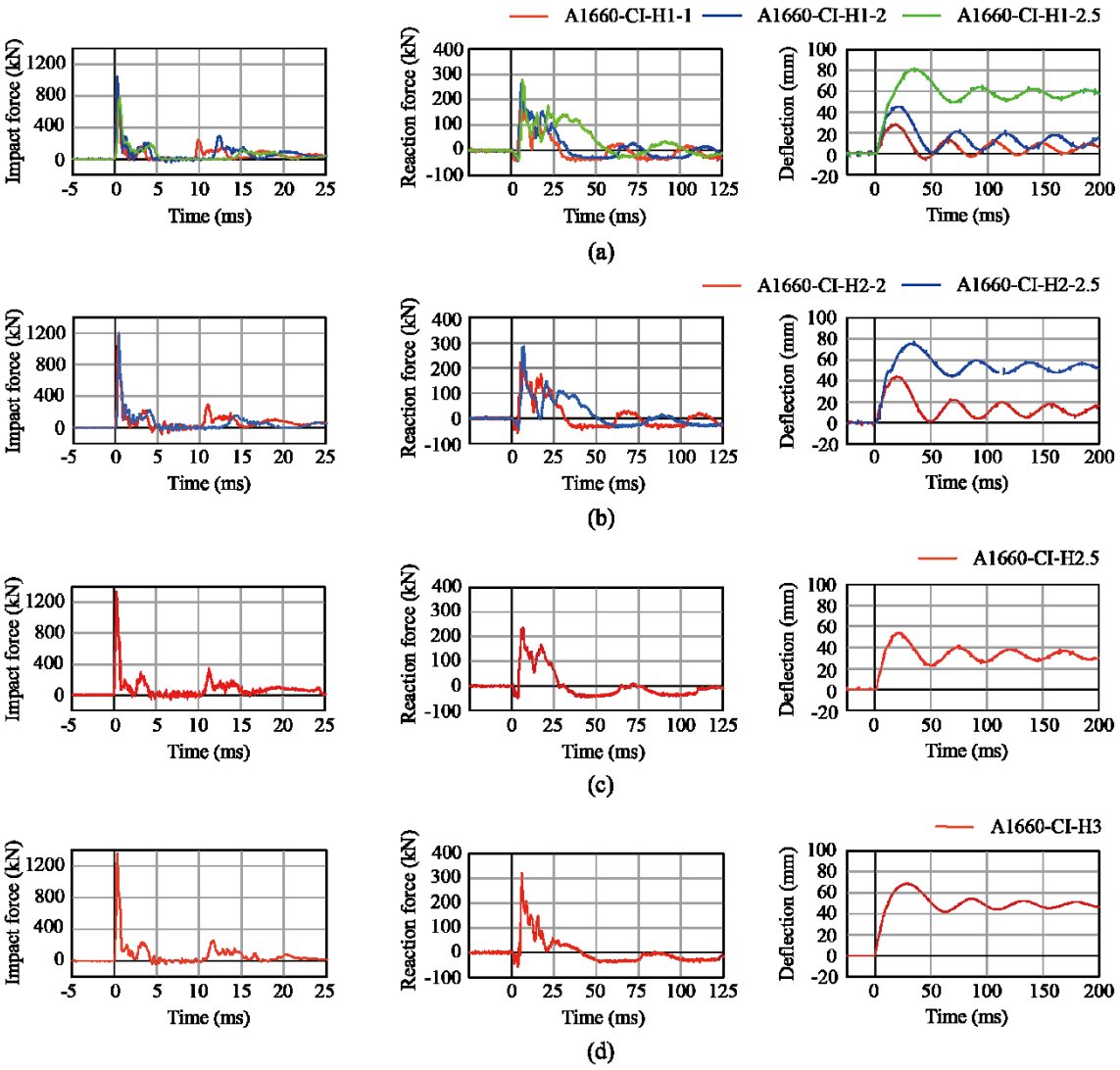

Figure 6.4. Comparisons of Beam A1660's impact force *P*, reaction force *R*, and deflection *D* time histories [53]: (a) Beam A1660-CI-H1; (b) Beam A1660-CI-H2; (c) Beam A1660-CI-H2.5; and (d) Beam A1660-CI-H3.

Figure 6.4 compares the time histories for each Beam A1660's dynamic responses during several loading steps.

Comparisons of the experimental findings for Beam A1660-CI-H1 are shown in Figure 6.4a. The results are shown in this figure, which show that: 1) the minimum and maximum impact forces excited at the drop heights H = 1.0 m and H = 2.0 m were 766 kN and 1047 kN, respectively; 2) the maximum reaction force tends to increase with increasing the drop height H even though the maximum impact force at H = 2.5 m was less than that at H = 2.0 m; and 3) as a result of the sheet debonding, the reaction force R's major response time at H=2.5 m was 25 ms longer than it was at H=2 m.

The maximum and residual deflections for each loading step grew with increasing the subsequent drop height *H*, and the natural duration of the damped-free vibration also lengthened correspondingly, according to the results of the deflection time histories. Even though the AFRP sheet debonded at the 2.5 m drop height, the effect was not immediately apparent in the time history. The sheet may have debonded at this loading phase, as evidenced by the fact that the residual deflection at H = 2.5 m increased by a factor of roughly five relative to that at H = 2 m.

Experimental findings for Beam A1660-CI-H2 are contrasted in Figure 6.4b. In this instance, AFRP sheet debonding caused the beam to attain its final state at the drop height H = 2.5 m. The following conclusion can be drawn from these data: 1) As the drop height *H* grew, both the maximum impact and reaction forces also increased; 2) as a result of the AFRP sheet debonding, the major response's time length at H = 2.5 m was 20 ms longer than it was at H = 2.0 m. When the maximum and residual deflections at the drop heights H = 2.0 and 2.5 m are compared between Beam A1660-CI-H1 (see Figure 6.4a) and Beam A1660-CI-H2, it can be seen that: 1) in the case of H = 2 m (A1660-CI-H1-2 and A1660-CI-H2-2), maximum and residual deflections are roughly the same to each other; however, 2) in the case at H = 2.5 m (A, Therefore, despite the FRP sheet that is used to strengthen the beams in their flexure, damage may still develop over time as a result of repeated loading.

Figure 6.4c displays the Beam A1660-CI-H2.5 experimental findings. In this instance, the AFRP sheet debonded during the initial loading stage, which caused the impact test to end after the initial load was delivered. The maximum reaction force remained at roughly 238 kN, while the maximum impact force was estimated to be around 1,346 kN. When compared to Beam A1660-CI-H1-2.5 and Beam A1660-CI-H2-2.5, respectively, the impact and response forces for Beam A1660-CI-H2.5 were greater.

According to the results of deflection time histories, the maximum and residual deflections for Beam A1660-CI-H2.5 significantly decreased when compared to those for Beams A1660-CI-H1-2.5 and A1660-CI-H2-2.5. This shows that in the instances of Beams A1660-CI-H1/2.5, the damage accumulated as a result of repeated loading.

The experimental outcomes for Beam A1660-CI-H3 are shown in Figure 6.4d. When the dynamic responses of Beams A1660-CI-H2.5/3 are compared, it can be seen that: 1) Beam A1660-CI-H3 had a slightly higher maximum reaction force and impact force than Beam A1660-CI-H2.5; 2) Despite having a trapezoidal shape, the major reaction force response for Beam AS-CI-H2.5 changed to a triangular shape for Beam

A1660-CI-H3; and 3) the deflection's dynamic response characteristics, with the exception of the maximum and residual deflections and the unloaded structure's inherent period of damped-free vibration, were similar to one another.

6.3.2 Crack patterns of RC beams

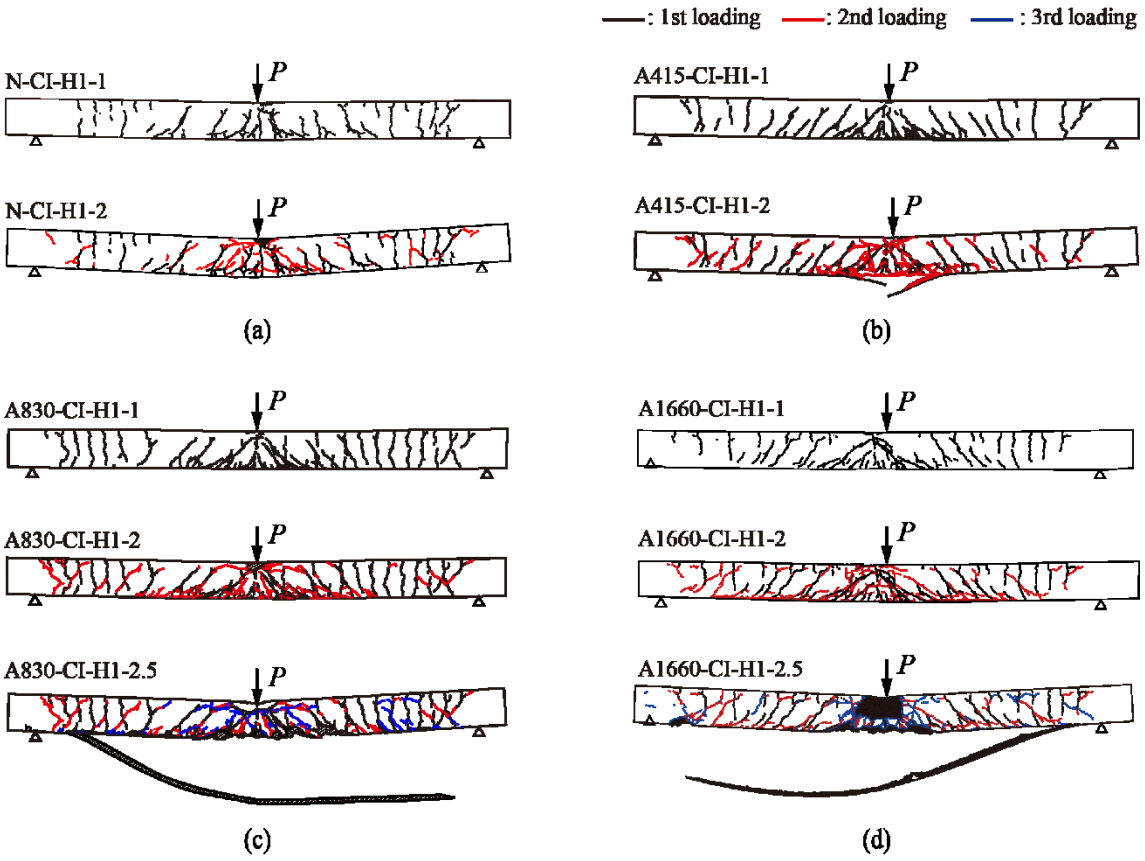

Figure 6.5. Crack patterns after consecutive impact loading:
(a) Beam N-CI-H1; (b) Beam A415-CI-H1;
(c) Beam A830-CI-H1; and (d) Beam A1660-CI-H1.

The beams with/without strengthening (Beam N-CI-H1 and Beam AS-CI-H1) are compared in Figure 6.5 for crack patterns following successive loading steps, with drop height H = 1 m of initial load. Because the beam was badly folded around the loading area at this loading level, Beam N-CI-H1 was surcharged to consecutive loading up to the H = 2.0 m in these figures. The information below can be seen from this figure: 1) the diagonal and flexural cracks that appeared on the beams after impact loading; 2) a fixed beam with a limited spanning length was built, causing flexural waves to propagate until they reached the support points, causing fractures to form from the top surface toward the

bottom; 3) regardless of the presence or absence of strengthening, the vicinity of the loading point was harmed in conjunction with the compression failure; 4) the strengthening effect of the AFRP sheet caused Beams AS to be less deformed than Beams N, despite Beams N being permanently distorted close to the loading point; 5) at drop height H = 2.0 m (second loading step), Beam A415 attained its ultimate condition, with the AFRP sheet rupturing; 6) in contrast, Beams A830 and A1660 attained their final state when the AFRP sheet debonded at a drop height of H = 2.5 m (third loading step); 7) whether or not they were reinforced with AFRP sheets, all RC beams failed with a flexural-shear failure mode.

According to Figure 6.5 and Table 6.1, the enhanced RC beams failed with sheet rupture when the sheet volume was relatively little (Beam A415), and they failed with sheet debonding when the sheet volume was quite big (Beams A830/1660). It suggests that the sheet tends to debond more quickly the larger the sheet volume.

6.3.3 Relationship between maximum response values and input impact energy

Figure 6.6 shows relationships between the absolute maximum deflection and the accumulated input impact energy E_{ai} and between the absolute residual deflection and the accumulated input impact energy E_{ai}. In these figures, the marks filled in white mean that the AFRP sheet debonded or ruptured.

In the case of Beam A415, it can be observed that the absolute maximum and residual deflections for all Beams AS under consecutive loading may be linearly distributed including the cases of the sheet rupturing. Even though those for unreinforced Beams N were also linearly distributed, the gradient for Beams AS was smaller than that for Beams N. Also, the AFRP sheet did not rupture until the accumulated input impact energy E_{ai} was greater than about 8.5 kJ for Beam A415-CI-H3.

The absolute maximum deflections for all beams subjected to sequential loading, including occurrences of sheet debonding, may have a linear distribution, as seen in the case of Beam A830. The following conclusions can be drawn from the results for absolute residual deflections as illustrated in Figure 6.6b: 1) the residual deflections for Beams AS, which do not include events in which the AFRP sheet debonded and had a linear distribution; 2) for the example of the drop height of H = 2.0 m for the Beam A830-CI-H1, the AFRP sheet did not debond until the total input impact energy Ea was greater than approximately 8.6 kJ; and 3) by properly reinforcing the beams using an AFRP sheet, the residual beam deflections can be significantly reduced.

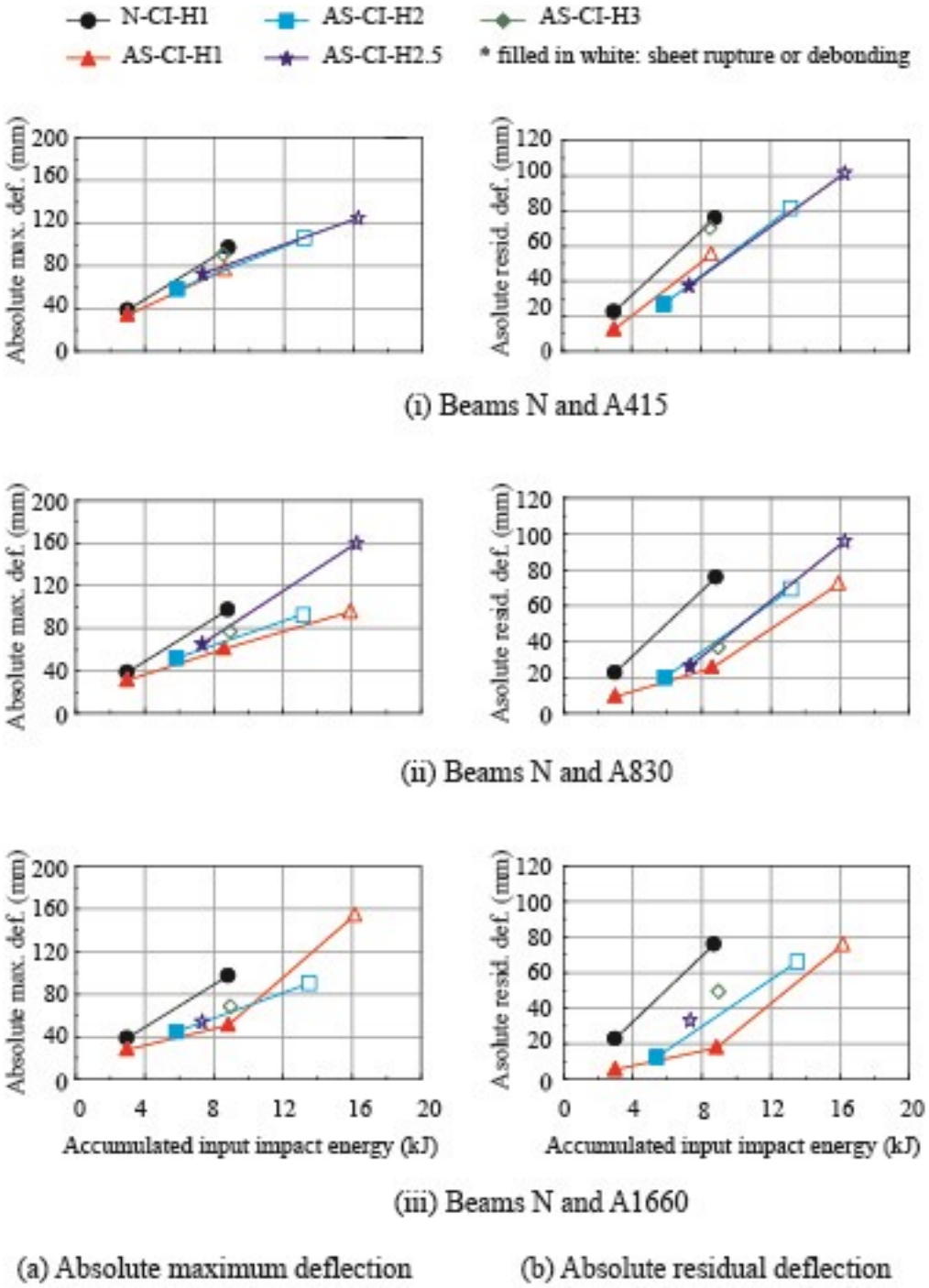

Figure 6.6. Relationship between absolute maximum response values and accumulated input impact energy E_{ai}.

When all Beams AS are subjected to consecutive impact loads, it is demonstrated in the case of Beam A1660 that the absolute maximum and residual deflections may be linearly distributed, with the exception of situations where the sheet is debonded. The sheet debonding also caused all reinforced RC beams to fail. The sheet separated from the beam when the input impact energy for Beam A1660-CI-H2.5 reached about 7.33 kJ,

but it did not separate from the beam when the total input impact energy exceeded 8.82 kJ for Beam A1660-CI-H1 at H = 2.0 m.

6.4 Summary

In this chapter, RC beams reinforced with AFRP sheet underwent repeated drop-weight impact loading tests. At each loading phase in this investigation, the input impact energy was steadily increased. These were the findings of this study:

1. In comparison to an unreinforced beam, strengthened beams' maximum and residual deflections were much better.

2. The reinforced beams' absolute maximum deflections were linearly distributed in relation to the total input impact energy.

3. Until the FRP sheet debonded, absolute residual deflections of the strengthened beams were also linearly distributed, correlating to an accumulation of input impact energy.

4. The final condition of the RC beams strengthened with the AFRP sheet, which had densities of 830 and 1660 g/m^2, was attained after the sheet debonded. The reinforced RC beams collapsed when the AFRP sheet with a volume of 415 g/m^2 ruptured. These failure types exhibit the same propensity as in the case of the single impact loading.

5. Whether or not they were reinforced with AFRP sheets, all RC beams collapsed with a flexural-shear failure mechanism.

Chapter 7: SUMMARY AND CONCLUSIONS

7.1 Summary

Twenty-five RC beams in total, including four unreinforced beams and twenty-one beams enhanced in flexure using the AFRP sheet bonding method, were examined in this study. Specimens were split up into various experimental groups according to the study's goal.

To examine the beams' load-bearing capacity, strain distribution, crack distribution, and failure behavior; to compare these findings with the outcomes of impact loading tests and analytical predictions, and to confirm the failure mode criterion of strengthened beams in comparison to earlier research. On the RC beams strengthened in flexure with externally bonded AFRP sheets, static loading studies were performed. Sheet volumes of 415, 830, and 1660 g/m^2 were employed. As a reference, unreinforced beams were also examined.

Drop-weight impact loading tests were performed on RC beams reinforced with AFRP sheets in order to examine the impact resistant behavior, including the strengthening effect and the failure modes of the flexure-strengthened RC beams with FRP sheets. The sheet volume was changed from 415 to 1660 g/m^2 to examine the effect of the sheet volume on the failure mode of the beams. The impact force was produced by dropping a 300 kg steel weight into the midspan of the beams from various heights (0.5, 1.0, 2.0, 2.5, 3.0, and 3.5m), and the drop height of the weight was raised until the sheets were debonded or ruptured. In contrast with strengthened beams, unreinforced beams were also put to the test.

Consecutive drop-weight impact loading tests on the RC beams enhanced in flexure with externally bonded AFRP sheets were also carried out in order to study the impact-resistant properties of the RC members. To assess the strengthening effect of beams, the sheet volume and the total input impact energy were looked at. The sheet volumes employed were 415, 830, and 1660 g/m^2. The weight's drop height was increased in steps 1.0, 2.0, 2.5, and 3.0 m up to the equivalent final state of the beam. Additionally examined as control beams were unreinforced beams.

Section 7.2 will provide an overview of all the findings from the aforementioned investigations.

7.2 Conclusions

7.2.1 Static behavior and failure mode of strengthened RC beams

The failure modes of the RC beams strengthened with AFRP sheets were investigated in this chapter utilizing static loading experiments employing the sheet volume. The conclusions are summarized as follows:

1. When compared to non-strengthened beams, the strengthened beams' capacity to carry loads was greatly increased.

2. Based on the predicted bending moment capacity ratio M_y/M_u, the failure mechanism of flexural strengthened RC beams was divided into two types: flexural compression failure and debonding failure. These findings are fairly consistent with the earlier investigation [21].

3. Flexural failure was the mode of failure for all RC beams, strengthened or not.

7.2.2 Low -velocity drop-weight impact loading tests

This chapter concentrated on using FRP materials to improve current RC constructions' impact resistance. In order to investigate the enhancement of impact-resistant beams and/or to forecast the failure modes of the RC beams strengthened with AFRP sheets, drop-weight impact loading experiments were carried out. Each beam underwent a single loading procedure for the impact loading tests, and the weight drop height was increased until the sheets broke or debonded. In order to assess the impact of utilizing FRP materials on the flexural strengthening of the RC beams, three different types of AFRP sheets with varying volumes were tested and externally attached to the bottom surfaces of the beams. The results are summarized as follows:

1. Based on the findings of the impact loading test, the maximum and residual displacement of the strengthened beams can be limited by up to 35% and 85%, respectively, in comparison to non-reinforced beams.

2. The maximum/residual displacement of the RC beams with/without AFRP sheets rose linearly when impact energy was added.

3. Based on the volume of the sheets, the failure mode of the reinforced RC beams was divided into two types: sheet rupturing and sheet debonding. The former is equivalent to the failure mode for flexural compression, whereas the latter is equivalent to the failure mode for debonding under static loading.

4. Whether or not the RC beams were strengthened with AFRP sheets, the failure mechanism of RC beams shifted from flexural failure under static loading to flexural-shear failure when subjected to impact loading.

5. Regardless of static or impact loads, increasing the sheet volume might not help the debonding of the AFRP sheet of the reinforced RC beams.

6. When the input impact energy was more than or equal to 7.33 kJ (corresponding to the drop height H = 2.5 m), the strengthened beams under test failed due to sheet debonding and/or rupturing.

7.2.3 Consecutive drop-weight impact loading tests

In this chapter, RC beams reinforced with AFRP sheet underwent repeated drop-weight impact loading tests. At each loading phase in this investigation, the input impact energy was steadily increased. These were the findings of this study:

1. In comparison to an unreinforced beam, strengthened beams' maximum and residual deflections were much better.

2. The reinforced beams' absolute maximum deflections were linearly distributed in relation to the total input impact energy.

3. Until the FRP sheet debonded, absolute residual deflections of the strengthened beams were also linearly distributed, correlating to an accumulation of input impact energy.

4. The final condition of the RC beams strengthened with the AFRP sheet, which had densities of 830 and 1660 g/m^2, was attained after the sheet debonded. The reinforced RC beams collapsed when the AFRP sheet with a volume of 415 g/m^2 ruptured. These failure types exhibit the same propensity as in the case of the single impact loading.

5. Whether or not they were reinforced with AFRP sheets, all RC beams collapsed with a flexural-shear failure mechanism.

REFERENCES

1. American Concrete Institute; ACI Committee 440. *Guide for the Design and Construction of Externally Bonded FRP Systems for Strengthening Concrete Structures*; American Concrete Institute: Farmington Hills, Mich., 2017; ISBN 978-1-945487-59-0.
2. Buchan, P.A.; Chen, J.-F. Blast Resistance of FRP Composites and Polymer Strengthened Concrete and Masonry Structures – A State-of-the-Art Review. *Compos. Part B Eng.* **2007**, *38*, 509–522, doi:10.1016/j.compositesb.2006.07.009.
3. Muszynski, L.; Purcell, M. Composite Reinforcement to Strengthen Existing Concrete Structures against Air Blast. *J. Compos. Constr.* **2003**, *7*, doi:10.1061/(ASCE)1090-0268(2003)7:2(93).
4. Pham, T.; Hao, H. Review of Concrete Structures Strengthened with FRP Against Impact Loading. *Structures* **2016**, *7*, doi:10.1016/j.istruc.2016.05.003.
5. Seyyed Mohammad Banijamali; Mohammad Reza Esfahani; Shoeib Nosratollahi; Mohammad Reza Sohrabi; Seyyed Roohollah Mousavi. Reviewing the FRP Strengthening Systems. *Am. J. Civ. Eng.* **2015**, *3*, 38–43, doi:10.11648/j.ajce.s.2015030202.18.
6. Norimitsu Kishi, Masato Komuro, Yusuke Kurihashi, Hiroshi Mikami Falling-Weight Impact Test of FRP Rods NSM RC Beams. In *5th International Conference on Protective Structures Poznan, Poland, August 20-24, 2018*; Poznan University of Technology: Poznan, Poland, 2018; Vol. Vol.5, p. pp.61-67.
7. Sharaky, I.A.; Torres, L.; Comas, J.; Barris, C. Flexural Response of Reinforced Concrete (RC) Beams Strengthened with near Surface Mounted (NSM) Fibre Reinforced Polymer (FRP) Bars. *Compos. Struct.* **2014**, *109*, 8–22, doi:10.1016/j.compstruct.2013.10.051.
8. Khalifa, A.M. Flexural Performance of RC Beams Strengthened with near Surface Mounted CFRP Strips. *Alex. Eng. J.* **2016**, *55*, 1497–1505, doi:10.1016/j.aej.2016.01.033.
9. Lee, H.Y.; Jung, W.T.; Chung, W. Flexural Strengthening of Reinforced Concrete Beams with Pre-Stressed near Surface Mounted CFRP Systems. *Compos. Struct.* **2017**, *163*, 1–12, doi:10.1016/j.compstruct.2016.12.044.

10. Al Rjoub, Y.S.; Ashteyat, A.M.; Obaidat, Y.T.; Bani-Youniss, S. Shear Strengthening of RC Beams Using Near-Surface Mounted Carbon Fibre-Reinforced Polymers. *Aust. J. Struct. Eng.* **2019**, *20*, 54–62, doi:10.1080/13287982.2019.1565617.
11. Abdallah, M.; Al Mahmoud, F.; Boissière, R.; Khelil, A.; Mercier, J. Experimental Study on Strengthening of RC Beams with Side Near Surface Mounted Technique-CFRP Bars. *Compos. Struct.* **2020**, *234*, 111716, doi:10.1016/j.compstruct.2019.111716.
12. Saadah, M.; Ashteyat, A.; Murad, Y. Shear Strengthening of RC Beams Using Side near Surface Mounted CFRP Ropes and Strips. *Structures* **2021**, *32*, 380–390, doi:10.1016/j.istruc.2021.03.038.
13. Imjai, T.; Setkit, M.; Figueiredo, F.P.; Garcia, R.; Sae-Long, W.; Limkatanyu, S. Experimental and Numerical Investigation on Low-Strength RC Beams Strengthened with Side or Bottom near Surface Mounted FRP Rods. *Struct. Infrastruct. Eng.* **2022**, 1–16, doi:10.1080/15732479.2022.2045613.
14. Cho, S.; Lee, H.; Chung, W. Strengthening Effect of Prestressed Near-Surface Mounted CFRP Bar System According to Material Properties of Aged Reinforced Concrete Beams. *Compos. Struct.* **2022**, *282*, 115121, doi:10.1016/j.compstruct.2021.115121.
15. Carolin, A. Carbon Fibre Reinforced Polymers for Strengthening of Structural Elements, Luleå tekniska universitet, 2003.
16. Ahmed, A.; Guo, S.; Zhang, Z.; Shi, C.; Zhu, D. A Review on Durability of Fiber Reinforced Polymer (FRP) Bars Reinforced Seawater Sea Sand Concrete. *Constr. Build. Mater.* **2020**, *256*, 119484, doi:10.1016/j.conbuildmat.2020.119484.
17. Shakir Abbood, I.; Odaa, S. aldeen; Hasan, K.F.; Jasim, M.A. Properties Evaluation of Fiber Reinforced Polymers and Their Constituent Materials Used in Structures – A Review. *Int. Conf. Adv. Mater. Behav. Charact. ICAMBC 2020* **2021**, *43*, 1003–1008, doi:10.1016/j.matpr.2020.07.636.
18. Philip A. Ritchie, D.A.T., Le-Wu Lu, and Guy M. Conelly. External Reinforcement of Concrete Beams Using Fiber Reinforced Plastics. *ACI Struct. J.* **1991**, *88*, doi:10.14359/2723.
19. Saadatmanesh, H.; Ehsani, M.R. RC Beams Strengthened with GFRP Plates. I: Experimental Study. *J. Struct. Eng.* **1991**, *117*, 3417–3433, doi:10.1061/(ASCE)0733-9445(1991)117:11(3417).

20. Thanasis C. Triantafillou Shear Strengthening of Reinforced Concrete Beams Using Epoxy-Bonded FRP Composites. *ACI Struct. J.* **1998**, *95*, doi:10.14359/531.
21. Kishi, N.; Mikami, H.; Matsuoka, K.G.; Kurihashi, Y. Failure Behavior of Flexural Strengthened RC Beams with AFRP Sheet. In *FRPRCS-5: Fibre-reinforced plastics for reinforced concrete structures Volume 1*; Thomas Telford Publishing, 2001; pp. 87–95 ISBN 978-0-7277-3647-5.
22. Kishi, N.; Zhang, G.; Mikami, H. Numerical Cracking and Debonding Analysis of RC Beams Reinforced with FRP Sheet. *J. Compos. Constr.* **2005**, *9*, 507–514, doi:10.1061/ ASCE1090-0268 20059:6 507.
23. Ahmed, E.; Sobuz, H.R.; Sutan, N.M. Flexural Performance of CFRP Strengthened RC Beams with Different Degrees of Strengthening Schemes. *Int. J. Phys. Sci.* **2011**, *6*, 2229–2238, doi:10.5897/IJPS11.304.
24. Attari, N.; Amziane, S.; Chemrouk, M. Flexural Strengthening of Concrete Beams Using CFRP, GFRP and Hybrid FRP Sheets. *Non Destr. Tech. Assess. Concr.* **2012**, *37*, 746–757, doi:10.1016/j.conbuildmat.2012.07.052.
25. More, R.U.; Kulkarni, D.B. Flexural Behavioural Study on RC Beam with Externally Bonded Aramid Fiber Reinforced Polymer. *Int. J. Res. Eng. Technol. July* **2014**, *3*, 316–321, doi:10.15623/ijret.2014.0307054.
26. Chen, W.; Pham, T.M.; Sichembe, H.; Chen, L.; Hao, H. Experimental Study of Flexural Behaviour of RC Beams Strengthened by Longitudinal and U-Shaped Basalt FRP Sheet. *Compos. Part B Eng.* **2018**, *134*, 114–126, doi:10.1016/j.compositesb.2017.09.053.
27. Raval, C.; Shah, S.; Machhi, C. Experimental Study on Shear Behaviour of RC Beam Strengthened by AFRP Sheet. *Int. J. Res. Writ.* **2020**, *3*, 62–68, PDF Url: http://www.ijciras.com/PublishedPaper/IJCIRAS1630.pdf (Accessed: 28th June 2020).
28. Madotto, R.; Van Engelen, N.C.; Das, S.; Russo, G.; Pauletta, M. Shear and Flexural Strengthening of RC Beams Using BFRP Fabrics. *Eng. Struct.* **2021**, *229*, 111606, doi:10.1016/j.engstruct.2020.111606.
29. Panahi, M.; Zareei, S.A.; Izadi, A. Flexural Strengthening of Reinforced Concrete Beams through Externally Bonded FRP Sheets and near Surface Mounted FRP Bars. *Case Stud. Constr. Mater.* **2021**, *15*, e00601, doi:10.1016/j.cscm.2021.e00601.
30. Jumaat, M.Z.; Alam, M.A. Strengthening of RC Beams Using Externally Bonded Plates and Anchorages. *Aust. J. Basic Appl. Sci.* **2009**, *3*, 2207–2211.

31. Godat, A.; Hammad, F.; Chaallal, O. State-of-the-Art Review of Anchored FRP Shear-Strengthened RC Beams: A Study of Influencing Factors. *Compos. Struct.* **2020**, *254*, 112767, doi:10.1016/j.compstruct.2020.112767.
32. Mostofinejad, D.; Shameli, M. Performance of EBROG Method under Multilayer FRP Sheets for Flexural Strengthening of Concrete Beams. *Procedia Eng.* **2011**, *14*, 3176–3182, doi:10.1016/j.proeng.2011.07.401.
33. Mostofinejad, D.; Shameli, S.M. Externally Bonded Reinforcement in Grooves (EBRIG) Technique to Postpone Debonding of FRP Sheets in Strengthened Concrete Beams. *Constr. Build. Mater.* **2013**, *38*, 751–758, doi:10.1016/j.conbuildmat.2012.09.030.
34. Mostofinejad, D.; Mahmoudabadi, E. Grooving as Alternative Method of Surface Preparation to Postpone Debonding of FRP Laminates in Concrete Beams. *J. Compos. Constr.* **2010**, *14*, 804–811, doi:10.1061/(ASCE)CC.1943-5614.0000117.
35. Mostofinejad, D.; Tabatabaei Kashani, A. Experimental Study on Effect of EBR and EBROG Methods on Debonding of FRP Sheets Used for Shear Strengthening of RC Beams. *Compos. Part B Eng.* **2013**, *45*, 1704–1713, doi:10.1016/j.compositesb.2012.09.081.
36. Mostofinejad, D.; Hosseini, S.A.; Razavi, S.B. Influence of Different Bonding and Wrapping Techniques on Performance of Beams Strengthened in Shear Using CFRP Reinforcement. *Constr. Build. Mater.* **2016**, *116*, 310–320, doi:10.1016/j.conbuildmat.2016.04.113.
37. Kishi, N.; Komuro, M.; Kawarai, T.; Mikami, H. Low-Velocity Impact Load Testing of RC Beams Strengthened in Flexure with Bonded FRP Sheets. *J. Compos. Constr.* **2020**, *24*, 04020036, doi:10.1061/(ASCE)CC.1943-5614.0001048.
38. Kawarai, T.; Komuro, M.; Kishi, N.; Mikami, H.; Sinh, L.H. Experimental study on failure mode of RC beams strengthened with AFRP sheet under impact loading. *J. Struct. Eng. A* **2019**, *65A*, 901–911, in Japanese, doi:10.11532/structcivil.65A.901.
39. Erki M. A.; Meier U. Impact Loading of Concrete Beams Externally Strengthened with CFRP Laminates. *J. Compos. Constr.* **1999**, *3*, 117–124, doi:10.1061/(ASCE)1090-0268(1999)3:3(117).
40. Tang, T.; Saadatmanesh, H. Behavior of Concrete Beams Strengthened with Fiber-Reinforced Polymer Laminates under Impact Loading. *J. Compos. Constr. - J COMPOS CONSTR* **2003**, *7*, doi:10.1061/(ASCE)1090-0268(2003)7:3(209).

41. Pham, T.; Hao, H. Impact Behavior of FRP-Strengthened RC Beams without Stirrups. *J. Compos. Constr.* **2016**, *20*, doi:10.1061/(ASCE)CC.1943-5614.0000671.
42. Pham, T.; Hao, H. Behavior of Fiber-Reinforced Polymer-Strengthened Reinforced Concrete Beams under Static and Impact Loads. *Int. J. Prot. Struct.* **2016**, *8*, doi:10.1177/2041419616658730.
43. Cotsovos, D. A Simplified Approach for Assessing the Load-Carrying Capacity of Reinforced Concrete Beams under Concentrated Load Applied at High Rates. *Int. J. Impact Eng.* **2010**, *37*, 907–917, doi:10.1016/j.ijimpeng.2010.01.005.
44. Goldston, M.; Remennikov, A.; Sheikh, M. Experimental Investigation of the Behaviour of Concrete Beams Reinforced with GFRP Bars under Static and Impact Loading. *Eng. Struct.* **2016**, *113*, 220–232, doi:10.1016/j.engstruct.2016.01.044.
45. Rabinovitch, O. Dynamic Debonding in Concrete Beams Strengthened with Composite Materials. *Int. J. Solids Struct.* **2012**, *49*, 3641–3658, doi:10.1016/j.ijsolstr.2012.07.025.
46. Tang, T.; Saadatmanesh, H. Analytical and Experimental Studies of Fiber-Reinforced Polymer-Strengthened Concrete Beams under Impact Loading. *ACI Struct. J.* **2005**, *102*, 139–149, doi:10.14359/13539.
47. Zhan, T.; Wang, Z.; Ning, J. Failure Behaviors of Reinforced Concrete Beams Subjected to High Impact Loading. *Sixth Int. Conf. Eng. Fail. Anal.* **2015**, *56*, 233–243, doi:10.1016/j.engfailanal.2015.02.006.
48. White Timothy W.; Soudki Khaled A.; Erki Marie-Anne Response of RC Beams Strengthened with CFRP Laminates and Subjected to a High Rate of Loading. *J. Compos. Constr.* **2001**, *5*, 153–162, doi:10.1061/(ASCE)1090-0268(2001)5:3(153).
49. Wang, W. Flexural Behaviour of FFRP Wrapped CFRC Beams under Static and Impact Loadings. *Int. J. Impact Eng.* **2017**, *111*, doi:10.1016/j.ijimpeng.2017.08.010.
50. Liu, Y.; Jiang, Z.; Wen, H.M. Predicting Impact Induced Delamination of FRP Laminates. *Int. J. Impact Eng.* **2019**, *137*, 103436, doi:10.1016/j.ijimpeng.2019.103436.
51. Sinh, L.H.; Komuro, M.; Kawarai, T.; Kishi, N. Failure Modes of Reinforced Concrete Beams Strengthened in Flexure with Externally Bonded Aramid Fiber-Reinforced Polymer Sheets under Impact Loading. *Buildings* **2022**, *12*, 584, doi:10.3390/buildings12050584.
52. Kishi, N.; Komuro, M.; Kawarai, T.; Mikami, H. Experimental study on impact resistance behavior of flexural strengthened RC beams with AFRP sheet under

consecutive impact loading. *J. Struct. Eng. A* **2019**, *65A*, 964–974, in Japanese, doi:10.11532/structcivil.65a.964.

53. Le Huy, S.; Komuro, M.; Kishi, N.; Kawarai, T. Experimental Study on Dynamic Behaviors of Flexural Strengthened RC Beams with AFRP Sheet Having 1660 g/m 2 Mass Under Consecutive Impact Loading. In *EASEC16*; Springer, 2021; pp. 863–873.
54. Fujikake, K.; Soeum, S.; Matsui, T. CFRP Strengthened RC Beams Subjected to Impact Loading. *Perform. Mater. Struct. Extreme Cond.* **2017**, *210*, 173–181, doi:10.1016/j.proeng.2017.11.063.
55. Fibex. Material Properties for Unidirectional AFRP Sheets. 2014.
56. JIS K 7165. Plastics—Determination of Tensile Properties—Part 5; Test Conditions for Unidirectional Fibre-Reinforced Plastic Composites. 2008.
57. JSCE (Japan Society of Civil Engineers). *Standard Specification for Concrete Structures-2007 Design*; JSCE: Tokyo, Japan, 2007; ISBN ISBN 978-4-8106-0752-9.
58. JSCE (Japan Society of Civil Engineers). *Standard specification for concrete structures-2017 Design in Japanese*; JSCE: Tokyo, Japan, 2018; ISBN 978-4-8106-0777-2.
59. Kaklauskas, G.; Bacinskas, D.; Šitnkus, R. Deflection Estimates of Reinforced Concrete Beams by Different Methods. *Statyba* **1999**, *5*, doi:10.1080/13921525.1999.10531473.
60. Hamed E.; Rabinovitch O. Dynamic Behavior of Reinforced Concrete Beams Strengthened with Composite Materials. *J. Compos. Constr.* **2005**, *9*, 429–440, doi:10.1061/(ASCE)1090-0268(2005)9:5(429).